J. Fluid Mech. (1979), *vol.* 92, *part* 3, *pp.* 459–496
Printed in Great Britain

Domains and boundaries of non-stationary oblique shock-wave reflexions. 1. Diatomic gas

By G. BEN-DOR and I. I. GLASS

Institute for Aerospace Studies, University of Toronto,
Ontario, Canada M3H 5T6

(Received 29 August 1979 and in revised form 30 May 1978)

Interferometric data were obtained in the UTIAS 10×18 cm hypervelocity shock tube of oblique shock-wave reflexions in nitrogen at initial temperatures and pressures of about 300 K and 15 torr. The shock-Mach-number range covered was $2 \leqslant M_s \leqslant 8$ over a series of wedge angles $2° \leqslant \theta_w \leqslant 60°$. Dual-wavelength laser interferograms were obtained by using a 23 cm diameter field of view Mach–Zehnder interferometer. In addition to our numerous results the available data for nitrogen, air and oxygen obtained over the last three decades were also utilized. It is shown analytically and experimentally that in non-stationary flows seven domains exist in the (M_s, θ_w) plane where regular reflexion (RR), single-Mach reflexion (SMR), complex-Mach reflexion (CMR) and double-Mach reflexion (DMR) can occur. In addition, the transition boundaries between these regions were established. The experimental results from many sources substantiate the present analysis, and areas of disagreement which existed in the literature are now clarified and resolved. It is shown that real-gas effects have a significant influence on the size of the regions and their boundaries. The comprehensive, accurate and sensitive isopycnic data will form a base for comparing existing and future numerical analyses of such complex flows.

1. Introduction

When a planar moving incident shock wave encounters a sharp compressive corner in a shock tube, two processes take place simultaneously. The incident shock wave is reflected by the wedge surface, whereas the induced non-stationary flow behind it is deflected by the wedge corner. In the following, the first process will be referred to as shock-wave reflexion, the second as flow deflexion and the overall phenomenon as shock-wave diffraction. For a given gas the diffraction process depends on three factors: (1) Mach number of the incident shock wave M_s; (2) corner wedge angle θ_w; (3) initial gas pressure and temperature. Four different types of shock-wave reflexions now have been observed in shock-tube experiments. They are: regular (RR), single-Mach (SMR), complex-Mach (CMR) and double-Mach (DMR) reflexions. Illustrations of these four possible oblique shock-wave reflexions are shown in figure 1 (plate 1).

Although RR and SMR were first noticed by the distinguished physicist and philosopher E. Mach as early as 1878, almost no work was done in this field until the 1940s when von Neumann reinitiated the problem. An intensive investigation at Princeton University under the supervision of Prof. W. Bleakney finally led to the discovery of CMR by Smith (1945) and DMR by White (1951). Once these four types

0022-1120/79/4199-6620 $02.00

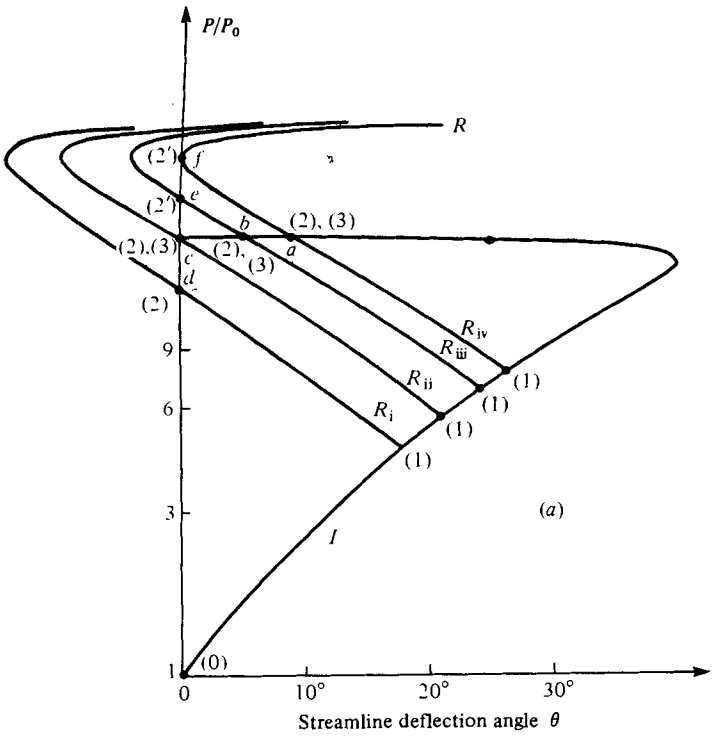

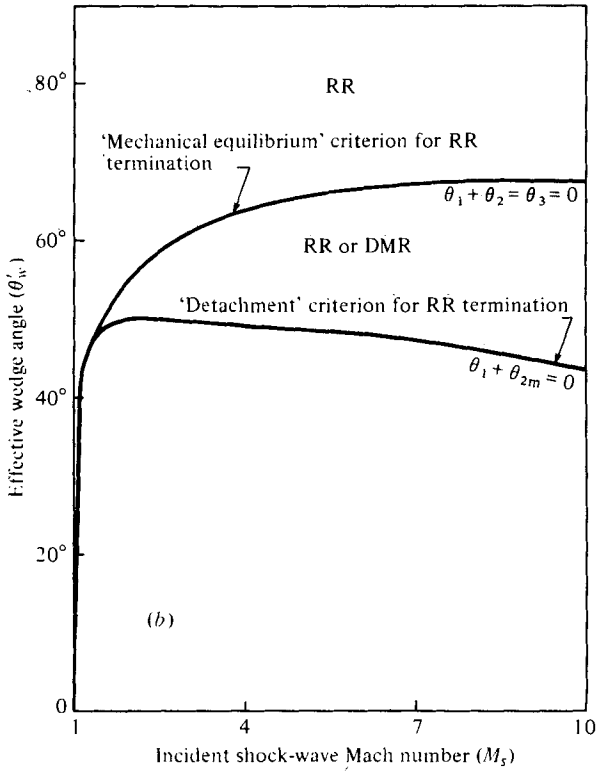

FIGURE 2(*a*, *b*). For legend see facing page.

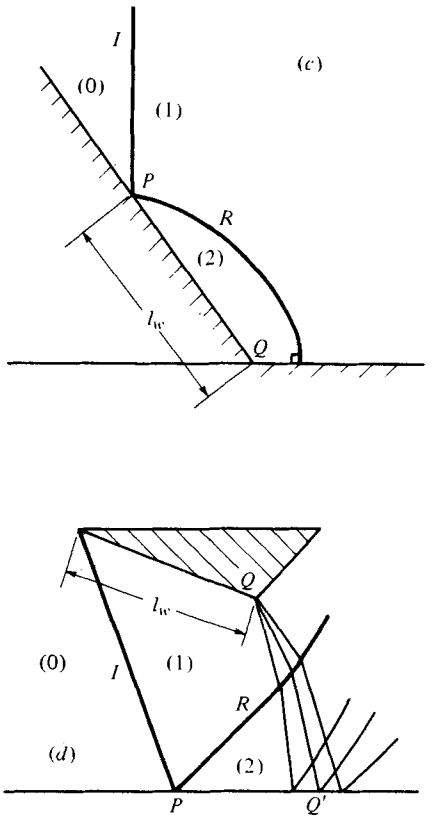

FIGURE 2. (*a*) Incident (*I*) and reflected (*R*) shock-polar combination illustrating different termination criteria for regular reflexion (RR). Imperfect nitrogen $M_0 = 4{\cdot}00$, $P_0 = 15$ torr, $T_0 = 300$ K. Various states are given by numbers in brackets. For clarity, letters *a*–*f* indicate transition paths corresponding to states shown by number. R_{i}: $\theta'_w = 60{\cdot}00°$, $M_s = 2{\cdot}00$. R_{ii}: 'mechanical-equilibrium' criterion, $\theta'_w = 56{\cdot}42°$, $M_s = 2{\cdot}21$. R_{iii}: $\theta'_w = 52{\cdot}66°$, $M_s = 2{\cdot}43$. R_{iv}: 'detachment' criterion, $\theta'_w = 49{\cdot}99$, $M_s = 2{\cdot}57$. Note: all polars are accurately drawn to scale for given conditions. (*b*) Comparison between the 'detachment' and the 'mechanical-equilibrium' criteria for RR termination in the (M_s, θ'_w) plane, imperfect nitrogen $P_0 = 15$ torr, $T_0 = 300$ K. Communication of a scale length l_w to the reflexion point *P*: (*c*) non-stationary flow; (*d*) steady flow.

of reflexion were found it became necessary to establish the transition criteria between them. The RR $\rightleftarrows$ SMR transition was first studied by von Neumann (1963) who assumed the following: (1) perfect gas; (2) two-dimensional inviscid flows; (3) when there are two possible solutions (the so-called weak and strong families of shock waves) for producing a required deflexion, the weak-shock solution will occur. This is an experimental fact which was verified in the study of two-dimensional supersonic wedge flows (Liepmann & Roshko 1957). Although an explanation of minimum entropy for weaker shocks is sometimes advanced it has not been proven analytically; and (4) the flow is pseudo-stationary. Using those assumptions von Neumann (1963) postulates that in a RR the streamline deflexion angle θ_2 through the reflected shock wave is equal in magnitude but opposite in sign to the deflexion angle θ_1 through the incident shock wave, i.e. $\theta_1 + \theta_2 = 0$. This is violated when the wedge angle θ_w decreases

to a point where it forces θ_1 to exceed the maximum deflexion angle θ_{2m}. This criterion will be referred to as the 'detachment' criterion. The detachment criterion can best be illustrated by using the pressure-deflexion (P, θ) shock polars. Consider figure 2(*a*) where the I and R polars represent the incident and reflected shock waves, respectively. Since the net deflexion through a RR is zero the solution is at the point where the R polar intersects the P/P_0 axis, i.e. state (2′ or *e*) on R_{III}. As the wedge θ_w decreases the R polar moves away from the P/P_0 axis until it becomes tangent to it [figure 2*a*, state (2′ or *f*) on R_{IV}]. With a further decrease in θ_w, the R polar will not intersect the P/P_0 axis any more and a RR is not possible. Consequently, the detachment criterion is represented by the R_{IV} shock polar.

Some disagreement between the detachment criterion and actual experiments were found by Smith (1945). In his experiments RR persisted beyond the limit determined by the detachment criterion. Kawamura & Saito (1956) who tried to resolve the disagreement by making use of shock polars discovered that the point of tangency between the R polar and the P/P_0 axis (i.e. R_{IV}, figure 2*a*) can lie outside or inside the I polar depending on whether the value of M_0 is greater or smaller than a certain change-over value M_{0c}. Unfortunately, their misprinted value for $M_0 = 3{\cdot}203$ does not match their other parameters $P_0/P_1 = 0{\cdot}433$, $\phi_0 = 41{\cdot}5°$ and $\gamma = 1{\cdot}4$ which results in $M_{0c} = 2{\cdot}198$. It is possible that the misprint should read 2·203, which is in good agreement with the above value. To compound the difficulty Henderson & Lozzi (1975) quote $M_{0c} = 2{\cdot}23$ for a perfect gas with $\gamma = 1{\cdot}402$ in the text, but unfortunately use the value of 2·40 in the caption to their figure 2. Using the value $\gamma = 1{\cdot}402$ we calculate $M_{0c} = 2{\cdot}192$. Molder (1979) has recently calculated for a perfect diatomic gas ($\gamma = 1{\cdot}4$) a value of $M_{0c} = 2{\cdot}202$. The value calculated here yields $M_{0c} = 2{\cdot}190$ ($M_s = 1{\cdot}450$ and $\theta'_w = 48{\cdot}55°$) for a perfect diatomic gas ($\gamma = \frac{7}{5}$) and $M_{0c} = 2{\cdot}185$ ($M_s = 1{\cdot}449$ and $\theta'_w = 48{\cdot}46°$) for imperfect nitrogen at $P_0 = 15$ torr and $T_0 = 300$ K. The significance of real-gas effects (vibration and vibration–rotation coupling) even at this low Mach number ($M_s \approx 1{\cdot}45$) is clear albeit small.

Henderson & Lozzi (1975) investigated the RR $\rightleftarrows$ SMR transition problem experimentally in a wind tunnel and in a shock tube. They introduced an alternative criterion which has the property that the system always remained in mechanical equilibrium (i.e. no pressure discontinuities) during transition. Consider figure 2(*a*) and note that, once RR terminates and SMR forms, the solution moves from the point where the R polar intersects the P/P_0 axis [state (2′ or *f*) on R_{IV}] to the point where the I and R polars intersect [states (2 and 3 or (*a*) on R_{IV}]. Consequently, a sharp pressure change is associated with this transition, if the detachment criterion is accepted and either M_s or θ_w are changed continuously so that the reflexion will go through transition conditions (i.e. start a RR and change to SMR or *vice versa*). Henderson & Lozzi (1975) argue that 'a system which develops a pressure discontinuity during transition cannot be in mechanical equilibrium' and that 'if a pressure discontinuity occurs during transition then an unsteady wave of finite amplitude or a finite amplitude band of waves will be generated in the flow. These would be expansion [waves] for RR → SMR and compression [waves] for SMR → RR.' However, since these waves have not been observed, they discarded the detachment criterion and suggested an alternative criterion that enables the system to be in mechanical equilibrium during transition. In order to maintain the system in mechanical equilibrium the transition should take place at the point where the R polar intersects the I polar (SMR) on the P/P_0 axis

(RR). This is illustrated by states (2) and (3 or c) on the R_{II} polar of figure 2(a). The formulation of this criterion yields $\theta_1+\theta_2=\theta_3=0$ (θ_3 is the deflexion of the flow while passing through the Mach stem) and it will be referred to as the 'mechanical-equilibrium' criterion. Consider polar R_{III} (figure 2a) and note that according to the detachment criterion a RR takes place at (2′ or e) while, according to the mechanical-equilibrium criterion, RR cannot occur, since the termination criterion given by R_{II} was exceeded. It is worth noting that the area of disagreement in the (M_s, θ'_w) plane ($\theta'_w=\theta_w+\chi$, where χ is the triple point trajectory angle) between these two criteria (figure 2b) is very large. The mechanical-equilibrium criterion rather than reducing the previously mentioned disagreement between theory and experiments found by Smith (1945), where RR occurred even below the line of the detachment criterion in shock-tube experiments at low incident shock wave Mach numbers, made it even worse, for their line lies above the detachment criterion line for all $M_s > 1{\cdot}68$ ($M_0 = 2{\cdot}23$, $\phi_0 = 41{\cdot}20°$). Nevertheless, Henderson & Lozzi should be credited for their new physical approach to the problem. It is possible that in an experiment where the wedge angle θ_w is changed gradually, perhaps one might obtain two different criteria for RR→SMR and SMR→RR transitions. Consider figure 2(a) and note that if one starts with a given SMR at states (2) and (3 or a) on R_{IV} and the wedge angle is increased slowly, it is conceivable that states a (SMR), b (SMR), c (SMR→RR) and d (RR) might be encountered, and hence the transition would follow the mechanical-equilibrium criterion. However, if one started with a given RR state (2 or d) on R_I and then decreases θ_w gradually, it is possible that the sequence of events might be states d (RR), c (RR), e (RR), f (RR) and a (SMR). This sequence of events follows the detachment criterion. Such experiments have not been made to date and need further study.

During their attempt to substantiate their mechanical-equilibrium criterion, Henderson & Lozzi (1975) found a 'remarkable anomaly' between their results from wind-tunnel and shock-tube experiments with single wedges where RR continued to exist below the detachment and mechanical-equilibrium transition boundary lines (figure 2b) in a region where the 'perfect-gas theory had no RR-solution'. This anomaly did not occur in non-stationary flows over double wedges or single concave corners. Henderson & Lozzi resolved the anomaly by postulating that those RR configurations found below the mechanical-equilibrium transition line were really undeveloped DMR configurations in which all shock waves, slipstreams and triple points typical of a well-developed DMR were too close together to be observed.

Since the disagreement concerning the RR ⇄ SMR transition could not be resolved analytically, Auld & Bird (1976) decided to approach the problem numerically. They studied the RR ⇄ SMR transition numerically in steady flows in the region where both types of RR and SMR are theoretically possible. Their calculations were carried out at the molecular level using the direct-simulation Monte-Carlo method. Since a RR was always established in the 'dual-solution region' in both monatomic and diatomic steady flows, Auld & Bird (1976) concluded that 'the recent conclusion [of Henderson & Lozzi (1975)] that Mach reflexion always occurs in the overlap region requires further study'; they suggested furthermore that 'low-density wind-tunnel results that resolved the wave structure of the reflexion point would be particularly useful'.

Hornung (1977) and Hornung, Oertel & Sandeman (1979) initiated another criterion for the termination of RR. They argued that in order for a SMR to form, a length scale

must be available at the reflexion point, i.e. pressure signals must be communicated to the reflexion point. This single argument eventually led them to two different termination lines for RR depending on whether the flow under consideration is steady or non-stationary.

Consider the non-stationary RR in figure 2(*c*) and note that the length l_w can affect the reflexion point P only when a subsonic flow is established between Q and P (in a frame of reference attached to P). In a steady flow [figure 2(*d*)] the length l_w can affect the reflexion point P only if a propagation path exists between point Q and point P via the expansion wave at Q'. This is possible only if the flow between P and Q' is subsonic. According to Hornung (1977) and Hornung *et al.* (1979) this could happen if a SMR existed since the flow behind the Mach stem is subsonic. Consequently, they argued that transition takes place the very first time a SMR can occur. Consider figure 2(*a*) and note that this corresponds to states (2) and (3) on R_{i1}, and represents the mechanical-equilibrium criterion of Henderson & Lozzi (1975). Thus, the analysis of Hornung *et al.* led to two different transition lines in steady and non-stationary flow. In steady flow the transition satisfies the mechanical-equilibrium criterion while for non-stationary flows their analysis led to a new transition line, which will be referred to as the 'sonic' criterion. Note that if the sonic-transition line were drawn in figure 2(*b*), it would coincide with the detachment-criterion-transition line since it lies slightly below it only at very weak incident shock waves. Hornung (1977) and Hornung *et al.* (1979) claim to have experimental data obtained in both shock-tube and wind-tunnel flows that verify their analysis.

Once RR terminates, three different types of reflexion can occur in non-stationary flows, i.e. SMR, CMR and DMR. White (1951, 1952) was the first to notice that when the flow behind the reflected shock wave, R, becomes supersonic in a frame of reference attached to the first triple point T (i.e. $M_{2T} > 1$) a kink forms in R and the transition SMR $\rightarrow$ CMR occurs. A mechanism for the transition was later suggested by Gvozdeva *et al.* (1969, 1970) and Henderson & Lozzi (1975). Henderson & Lozzi suggested that a 'band of compression waves' must exist in a CMR. These compression waves then converge to a shock wave to form a DMR when $M_{2T} > 1$. Unfortunately, their suggestion was not substantiated analytically or experimentally. In addition, the precise value of M_{2T} for the termination of CMR and the formation of DMR was not established either. The correct gasdynamic criterion for the transition CMR $\rightleftarrows$ DMR was established during the present study. It will be shown that the flow Mach number behind the reflected shock wave with respect to the 'kink' of a CMR M_{2K}, must be greater than unity (i.e. $M_{2K} > 1$) for a DMR to form. Consequently, the CMR $\rightleftarrows$ DMR transition occurs at $M_{2K} = 1$. It will be shown furthermore that in nitrogen $M_{2K} = 1$ corresponds to $M_{2T} \approx 1{\cdot}3$ and hence Gvozdeva *et al.* (1969, 1970) and Henderson & Lozzi (1975) were correct in predicting the transition at $M_{2T} > 1$. An attempt to establish some transition boundary lines experimentally was made by Bazhenova, Fokeev & Gvozdeva (1976). However, their experiments did not cover a significant range of incident shock wave Mach number (M_s) and corner wedge angles (θ_w). Their experimental boundaries for SMR, CMR and DMR are limited to $M_s < 4{\cdot}5$. Unfortunately, experiments by other researchers also did not cover a wide range of interest. Smith (1945), White (1951, 1952) and Kawamura & Saito's (1956) experimental data covered only the range $1 < M_s < 2{\cdot}75$, while Henderson & Lozzi's (1975) experiments were centred around the RR-termination criterion line. Law & Glass (1971)

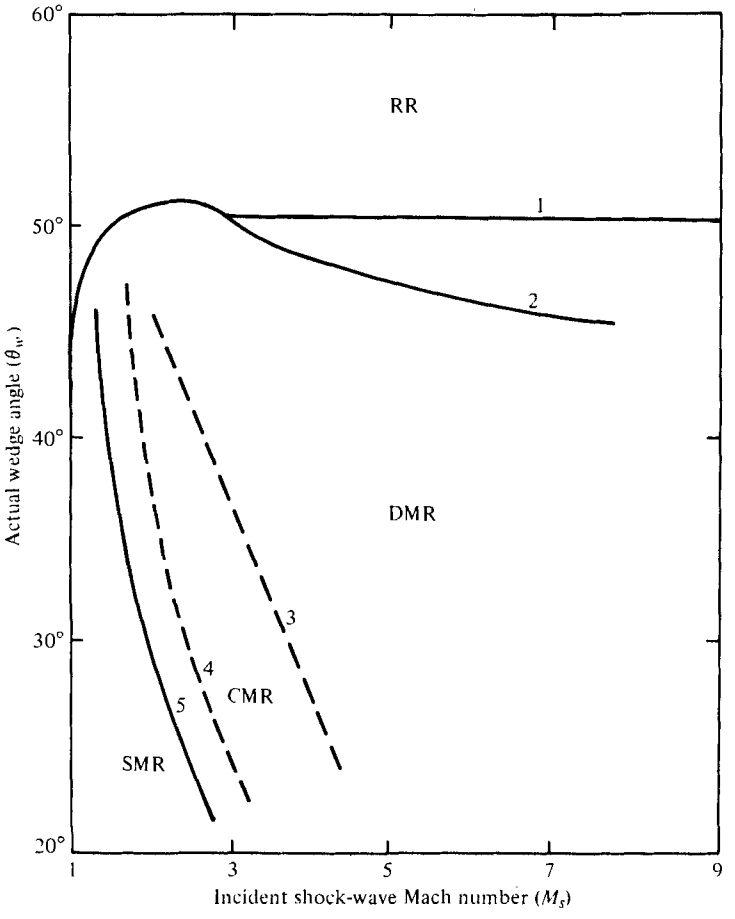

FIGURE 3. Domains and boundaries of shock wave reflexion in (M_s, θ_w) plane (enlarged reproduction of figure 5 from Bazhenova *et al.* 1976). ——, analytical; – – –, experimental.

were the first to extend the range of incident shock Mach numbers up to $M_s \leqslant 8$, but their corner wedge-angle range at the lower end was limited ($25° \leqslant \theta_w \leqslant 60°$).

Figure 3 is a reproduction of figure 5 from the paper by Bazhenova *et al.* (1976). It summarizes all the theoretical and experimental knowledge (excluding the mechanical-equilibrium criterion for the termination of RR, discussed earlier) concerning the regions and boundaries of RR, SMR, CMR and DMR which was available when the present study started. Only the termination criterion of RR is calculated analytically for both perfect and imperfect gases (lines 1 and 2, respectively). Although the SMR line is also calculated (line 5) for a perfect gas only, it does not start or terminate at any other boundary line and hence does not enclose any region. The imperfect boundary lines between SMR, CMR and DMR (lines 3 and 4) were all obtained experimentally and they do not encompass any closed region. There is no information about the types of reflexions for wedge angles in the range $0 < \theta_w \leqslant 20°$.

Although most of the investigators were interested in finding the correct transition criteria from one type of reflexion to another there were some attempts (Bargmann

1945; Fletcher & Taub 1951; Schneyer 1975; Kutler & Shankar 1977; Shankar, Kutler & Anderson 1977) to solve the entire flow field for a given reflexion utilizing various analytical or numerical methods. Unfortunately the numerical results suffer from a lack of agreement for the same initial conditions depending on the technique used for a solution (see Ben-Dor & Glass (1978) for details).

In view of the above literature survey the present research was directed towards the following.

(1) Resolving the disagreements concerning the termination of RR.

(2) Establishing the correct CMR $\rightleftarrows$ DMR transition criterion.

(3) Defining domains and transition boundaries of the various reflexions in order that they can be predicted *a priori*.

(4) Extending the experimental data over a much wider range, i.e. $0 \leqslant \theta_w \leqslant 60°$ and $1 \leqslant M_s \leqslant 8$.

(5) Resolving and clarifying areas of disagreement existing in the literature concerning this complex problem.

During the present study all the criteria for the formation and termination of RR, SMR, CMR and DMR were established analytically. Consequently, the (M_s, θ'_w) and the (M_s, θ_w) planes were divided into the domains of different types of reflexion and diffraction processes, respectively.

In analysing the shock-wave-reflexion problem two major difficulties arise: the nonlinearity of the equations of motion, and the inclusion of real-gas effects. These were overcome, and for the first time the 14 well-known oblique shock-wave equations of a SMR were solved for imperfect gases in dissociation equilibrium (Ben-Dor 1978*a*). It is shown that real-gas effects have a significant influence on the size of the different reflexion and diffraction domains and their transition boundaries.

Nearly 60 experiments were performed in the 10×18 cm UTIAS Hypervelocity Shock Tube in nitrogen, at an initial temperature of nearly 300 K and a pressure of 15 torr. The shock Mach number range was $2 \leqslant M_s \leqslant 8$ over a series of wedge angles $2° < \theta_w < 60°$. Dual-wavelength interferograms were obtained by using a 23 cm diameter field of view Mach–Zehnder interferometer equipped with a pulsed-laser source. For each and every type of diffraction the shock shapes and density field (isopycnics) as well as the density distribution along the wedge surface were deduced from the corresponding interferograms.

The experimental results of the present study and that of other sources substantiate the present analysis. In addition areas of disagreement which existed in the literature have been clarified and resolved.

The interferometric data on flow isopycnics presented here are the most comprehensive in the literature and the first since the pioneering experiments of White (1951) at very low shock Mach numbers. The isopycnics also form a solid data base to be used for comparison with analyses done by computational fluid dynamicists (Ben-Dor & Glass 1978). The isopycnics are far more sensitive to the numerical solutions than the predicted shock-wave-reflexion configurations. Undoubtedly, computer codes will evolve in the future and will be able to accurately predict all the inviscid flow properties of perfect and imperfect gases undergoing non-stationary oblique shock-wave reflexions.

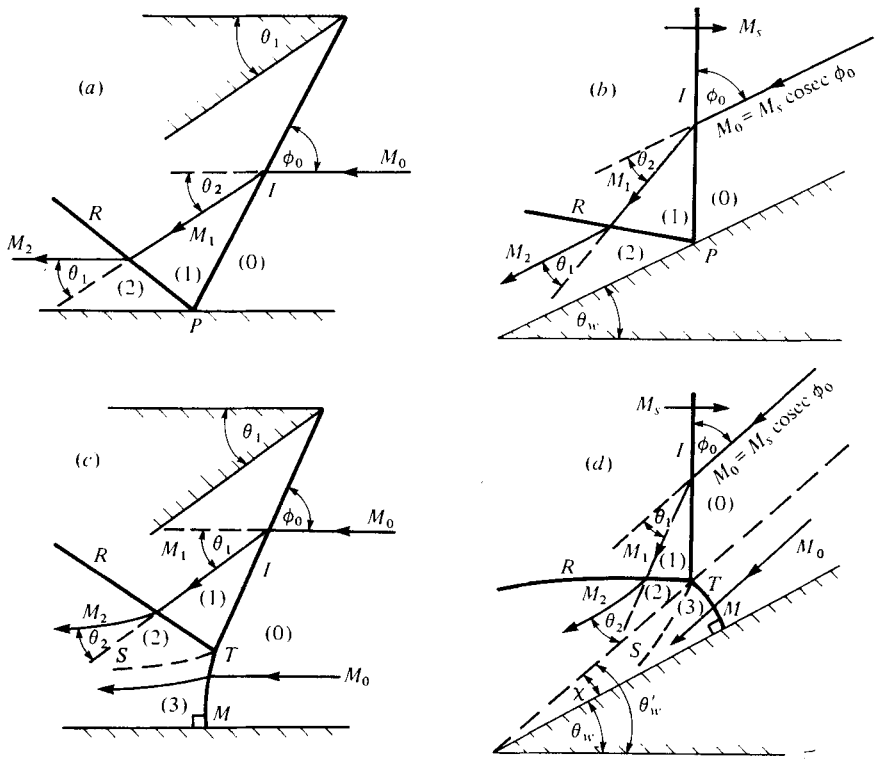

FIGURE 4. Equivalent oblique shock wave reflexions in steady and non-stationary flows. (*a*) Regular reflexion in steady flow. (*b*) Regular reflexion in non-stationary flow. (*c*) Single-Mach reflexion in steady flow. (*d*) Single-Mach reflexion in non-stationary flow.

2. Analysis

Since the incident shock wave moves with a constant velocity, the entire problem can be considered from a pseudo-stationary point of view, by attaching a frame of reference to any point on the incident shock wave. The above suggests that instead of three independent variables x, y and t the phenomenon is now describable in terms of x/t and y/t and the flow is self-similar.

In the pioneering analysis of Jones, Martin & Thornhill (1951) they showed that if a non-stationary reflexion is self-similar it can be made pseudo-stationary by superimposing a counterflow $M_0 = M_s \operatorname{cosec} \phi_0$ with respect to the point of reflexion P, parallel to the wall for the case of regular reflexion (compare figures 4*a* and 4*b*) and along the triple point path for single-Mach reflexion (compare figures 4*c* and 4*d*). This was substantiated experimentally by Parks (1952). The remaining cases of CMR and DMR can be treated in the same way although they have no steady-flow equivalent.

2.1. *Oblique shock-wave reflexion*

Reasons for reflexion. Steady RR and SMR can be viewed as arising from the boundary condition that the supersonic flow M_1 coming through the incident shock wave I must not collide with the wall (figures 4*a*, *c*). The analogous situation for non-stationary flows is shown in figure 5(*a*), where the frame of reference is attached to

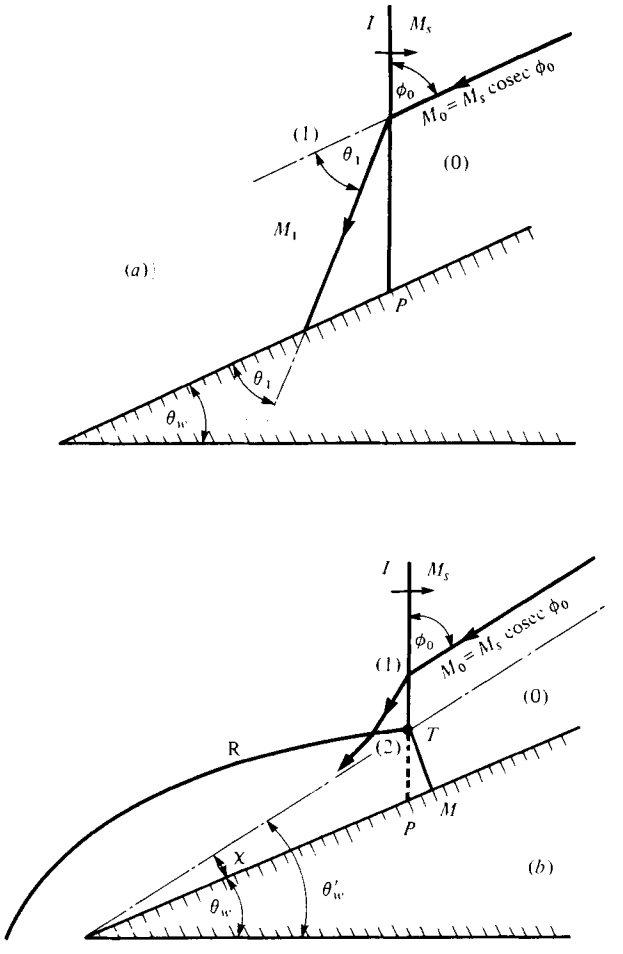

FIGURE 5. Explanatory diagrams of the reasons for non-stationary shock wave diffractions. (*a*) Non-stationary flow with $M_1 > 1$ with respect to point P. $\phi_0 = 90 - \theta_w$. (*b*) Non-stationary flow with $M_1 < 1$ with respect to point P. $\phi_0 = 90 - \theta'_w$, $\theta'_w = \theta_w + \chi$.

point P. As the weak solution usually takes place in steady flows, the angle of incidence ϕ_0 between the flow M_0 and the shock wave I (figures 4*a*, *c*) always lies in the range $\mu \leqslant \phi_0 < \phi_m$. Here μ is the Mach angle $\mu = \sin^{-1}1/M_0$ and ϕ_m is the incident angle corresponding to the maximum wedge-deflexion angle θ_m. A supersonic flow with $M_1 > 1$ (weak solution) always results behind I (figures 4*a*, *c*). In the non-stationary case, however, since $\phi_0 = 90° - \theta_w$ (figure 5*a*), ϕ_0 can also be in the range $\phi_m < \phi_0 \leqslant 90°$ by choosing the correct value of θ_w i.e. $0 \leqslant \theta_w < (90° - \phi_m)$. Consequently, the flow behind I is subsonic ($M_1 < 1$) with respect to point P (strong solution). This would suggest a no-reflexion situation in the non-stationary case. However, it is an experimental fact that, instead, a SMR occurs in this range of wedge angles ($0 < \theta_w \leqslant 90° - \phi_m$). We suggest that the reflexion (when $M_1 < 1$) arises from the interaction of the incident shock wave with the bow shock wave generated by the wedge (figure 5*b*). In a frame of reference attached to point T, where these two shock waves meet, state (2) results

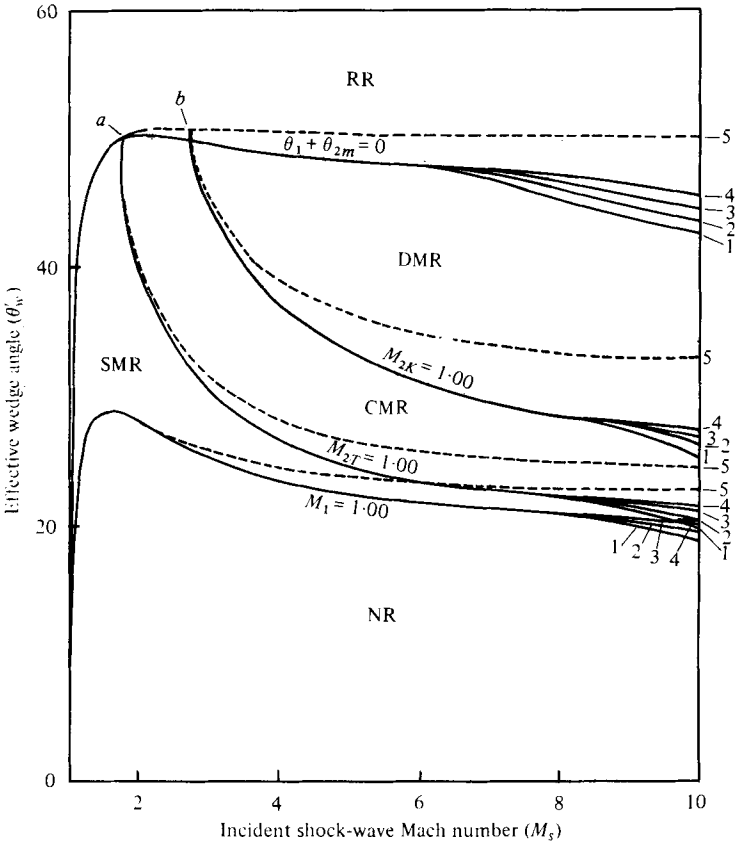

FIGURE 6. Regions of different oblique-shock wave reflexion in (M_s, θ'_w) plane. Lines 1–4 are for imperfect nitrogen with $P_0 = 1$, 10, 100 and 1000 torr, respectively, and $T_0 = 300$ K. Line 5 is for a perfect gas $\gamma = \frac{7}{5}$. RR, regular reflexion; SMR, single-Mach reflexion; CMR, complex-Mach reflexion; DMR, double-Mach reflexion; and NR, no reflexion.

from state (1) on passing through the bow shock R. Consequently, $P_2 > P_1$ and $P_2/P_0 > P_1/P_0$. To satisfy the last condition, the portion of the incident shock wave I that lies below T (dashed line TP) must move forward from P to M to be more normal to the oncoming relative flow, forming the Mach stem TM, triple point T and its trajectory angle χ, a slipstream S and state (3) (for simplicity neither is shown). All the SMR shown subsequently in figures 20 and 21 for $\theta_w = 2°$, 5°, 10° and 20° are cases where $M_1 < 1$ with respect to point P. Again one can conclude that here as well the weak solution occurs rather than the strong one. However, the strong solution does take place, but only for $\theta_w = 0$ ($\phi_0 = 90°$), i.e. a normal shock wave.

The angle χ plays a significant role when it makes $\theta'_w = \theta_w + \chi$ large enough to make $M_1 > 1$ with respect to the triple point T (see figure 6). When the induced flow behind the incident shock wave becomes subsonic ($M_{2'} < 1$), and no shock wave arises from its interaction with the corner neither of the two reasons for shock wave reflexions (figures 5*a*, *b*) applies. Consequently, it may be concluded that shock-wave reflexion in the non-stationary case additionally depends on the flow-deflexion process over the wedge corner. This is probably the reason for the existence of CMR and DMR in non-stationary flows in addition to RR and SMR found in steady flows.

Formation and termination criteria of RR, SMR, CMR and DMR. As noted earlier, three different criteria for the termination of RR exist in the literature. The first one is due to von Neumann (1963) and is known as the 'detachment' criterion. Analytically it is expressed as:

$$\theta_1 + \theta_{2m} = 0. \tag{1}$$

The second criterion, the 'mechanical-equilibrium' criterion, is due to Henderson & Lozzi (1975) and given by:

$$\theta_1 + \theta_2 = \theta_3 = 0. \tag{2}$$

The third criterion, due to Hornung (1977) and Hornung *et al.* (1979), is called the 'sonic' criterion or

$$\theta_1 + \theta_{2s} = 0. \tag{3}$$

Since the sonic point and the point of maximum deflexion are usually very close, it is impractical to distinguish between the 'sonic' and the 'detachment' criteria, and hence only the first two criteria will be considered here.

Hornung (1977) and Hornung *et al.* (1979) who introduced the 'sonic' criterion (3) claim that their analysis was substantiated by their experiments. Their data for non-stationary flow did not agree with the 'mechanical-equilibrium' criterion. One should also keep in mind the noted 'remarkable anomaly' found by Henderson & Lozzi (1975) in their non-stationary experiments with single wedges. A few experiments conducted in the present work in order to verify their suggestion of undeveloped DMR configuration (see § 1) using an optical magnification of 5·4 for $M_s \approx 4{\cdot}7$, $\theta_w = 60°$ and a wedge 8·5 cm long, failed to show any sign of DMR.

In all experiments claimed by Henderson & Lozzi (1975) to be undeveloped DMR configurations, the reflected shock wave R is straight near the reflexion point. This indicates that the flow behind R is supersonic ($M_2 > 1$) and hence parallel to the wall. However, a DMR should produce subsonic flow. Note also that Henderson & Lozzi's argument that the system must remain in mechanical equilibrium during transition is justified only if either M_s or θ_w are changed continuously to cause transition. However, for a given combination of M_s and θ_w (i.e. no changes in these parameters) the requirement of mechanical equilibrium appears unwarranted. Consequently, all the available evidence favours Hornung (1977) and Hornung *et al.*'s (1979) conclusion that the 'mechanical-equilibrium' criterion is inapplicable to non-stationary flows. Therefore, it can be concluded that the detachment criterion (1) is the correct criterion for the termination of RR in non-stationary flows.

The fact that Henderson & Lozzi (1975) obtained RR configurations beyond the detachment criterion line (calculated from perfect-gas theory) is resolved when real-gas effects are taken into account, as shown in figure 6. It is seen that the real-gas (solid) line ($\theta_1 + \theta_{2m} = 0$) starts to diverge from the perfect-gas line (dashed) at $M_s = 1{\cdot}47$, owing to vibrational excitation. At $M_s \sim 6$ it is about 2·5° below the perfect-gas line. From there on dissociation takes place and the line splits and the components (1–4) drop even further with decreasing initial pressure (for a fixed initial temperature). At $M_s = 10$ the lines that correspond to the initial pressures of 1000 (line 4) and 1 torr (line 1) lie at 4·7 and 7·4°, below the perfect-gas line.

The fact that real-gas effects shift the RR boundary line downwards (figure 6) even at very low Mach numbers (the shift at $M_s = 2{\cdot}5$ is 0·8° in effective wedge angle

θ'_w) can explain some of the disagreement found by Smith (1945), where RR was obtained below the terminating line. It is worth noting that his experiments were made in air where an even greater shift results, owing to the presence of about 20% oxygen, which becomes vibrationally excited at a lower shock Mach number than nitrogen.

It is worthwhile to briefly summarize the results of Smith (1945). He referred to shock waves as weak or strong depending on whether their Mach number M_s was smaller or greater than 1·46. His strong shock results revealed that RR persisted somewhat beyond the theoretical transition boundary calculated from the detachment criterion. Beside the fact that we have shown that real-gas effects start to become significant at $M_s = 1{\cdot}47$ for this boundary line Smith said that 'it seems likely that they [the discrepancies in the experimental results] lie in the experiment rather than in the theory'. He also reported that 'the front [of his shock waves] was somewhat curved' and 'the center of the front was usually slightly ahead of its ends and the angle between the upper and lower halves of the front was often as large as 0·5°'. In the case of weak shocks Smith reports that 'this angle was not over 0·2°' and that 'faint shocks behind and inclined to the main front are often visible' [see Glass, Martin & Patterson (1952) for an explanation]. He also claimed that 'from the intensities of their traces on the photographs, it is evident that their strengths are small compared to the main shock'. The origin of these 'satellite shocks' was correctly believed by Smith to 'arise in the breaking of the cellophane [diaphragm]'. In the case of very weak shock waves, $M_s \leqslant 1{\cdot}1$, Smith reported his experimental results to be in 'definite disagreement' with theory. On the other hand, the data obtained by Kawamura & Saito (1956) for $M_s = 1{\cdot}1$, did not agree with the results of Smith (1945). The discrepancy in the reflected shock angle was as much as 9°. It is important to note here that for very low Mach numbers the slope of the RR boundary line, i.e. $d\theta'_w/dM_s$ or $d\theta_w/dM_s$ is very high (see figure 6). Consequently, a small error in the measurement of M_s could explain some of the discrepancies reported by Smith. This remark becomes even more important if one recalls the fact that Smith (1945) reported the front of his shock waves were not completely formed when his photographs were taken. Consequently the incident shock wave was probably still accelerating (see Glass & Patterson, 1953) and did not have a constant velocity or Mach number. The method used by Smith to determine the value of M_s was far from satisfactory in our present context. Prior to his work he obtained an empirical curve of the form

$$P_{21} = P_2/P_1 = f(P_4/P_1),$$

where P_1 and P_2 are the pressures ahead of and behind the shock wave and P_4 is the actual breaking pressure of the diaphragm. Once this curve was obtained he translated the reading of P_4 (i.e. P_4/P_1) during his experiments to P_{21} according to his empirical curve and in turn calculated M_s from $M_s = [\beta(1+\alpha P_{21})]^{\frac{1}{2}}$, where $\beta = (\gamma-1)/2\gamma$, $\alpha = (\gamma+1)/(\gamma-1)$ and $\gamma = C_p/C_v$. In other words he did not measure the precise velocity of each shock wave in his experiments. Unfortunately, we were not able to perform experiments in the range $M_s < 2$. However, we would urge a repetition of Smith's experiments using presently available accurate methods of measuring velocity in order to finally obtain a reliable set of data in the low shock Mach number range of $1 \leqslant M_s \leqslant 2$.

The exact value of M_{0_c} for the termination criterion of RR, i.e. the case when the

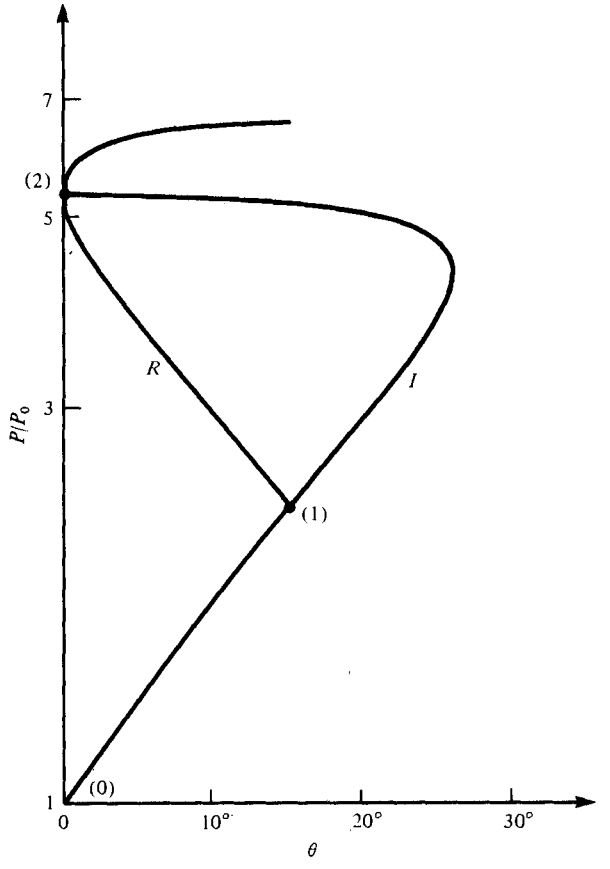

FIGURE 7. I and R polar combination for change-over Mach number M_{0c}, $\gamma = \frac{7}{5}$, $M_{0c} = 2{\cdot}190$, $M_s = 1{\cdot}450$, $\theta'_w = 48{\cdot}55°$.

R polar is exactly tangent to the P axis at the point where the I polar intersects it (figure 7) was not settled. The value calculated by us yields $M_{0_c} = 2{\cdot}185$ ($T_0 = 300\,\mathrm{K}$) for real nitrogen and $M_{0c} = 2{\cdot}190$ for a perfect diatomic gas ($\gamma = \frac{7}{5}$). The significance of real-gas effects even at these low Mach numbers ($M_s \approx 1{\cdot}45$) is clear, albeit small.

When RR terminates, three different types of reflexion, i.e. SMR, CMR and DMR, can occur depending on the Mach number of the flow behind the reflected shock wave R. As long as this flow is subsonic with respect to the first triple point T a SMR occurs. When this flow becomes supersonic with respect to T, a kink K forms in the reflected shock wave R, SMR terminates and a CMR forms. Consequently, the termination criterion for SMR and the formation criterion for CMR is

$$M_{2T} = 1. \tag{4}$$

CMR terminates when the flow behind R becomes supersonic with respect to the kink K. Therefore, the termination criterion for CMR and formation criterion of DMR is:

$$M_{2K} = 1. \tag{5}$$

It is worthwhile mentioning that the line $M_{2K} = 1$ corresponds approximately to $M_{2T} = 1{\cdot}3$ for nitrogen. Therefore, one may alternatively use the following empirical

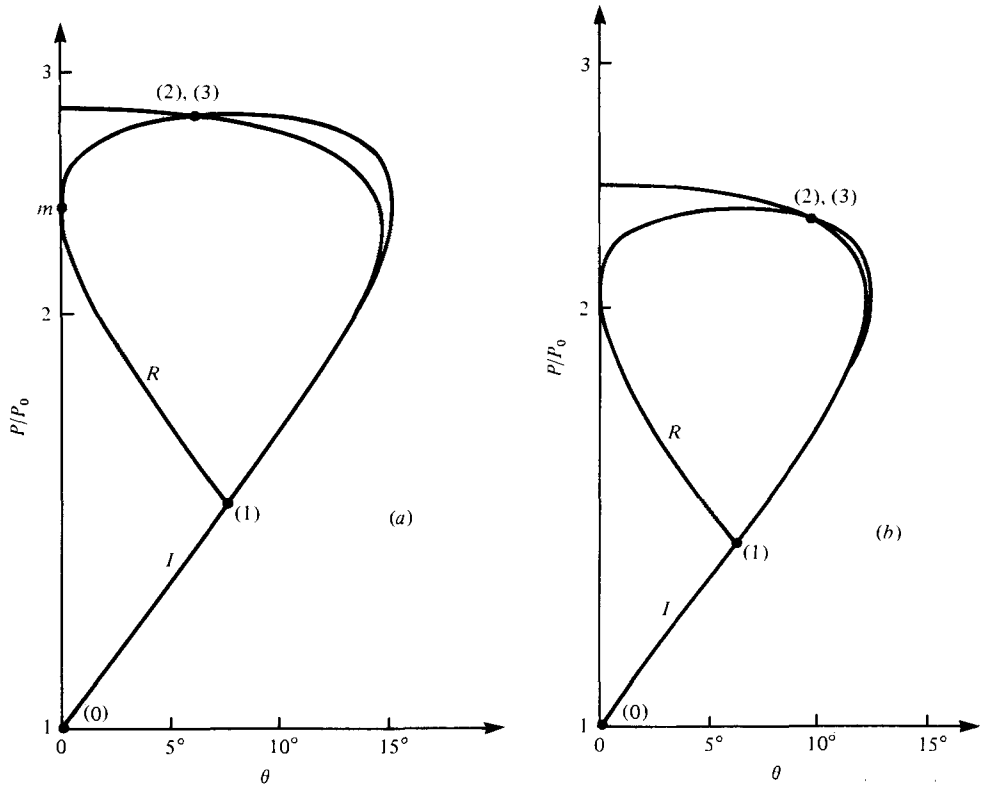

FIGURE 8. Shock polar illustration of two different families of single-Mach reflexion. (*a*) $\theta_3 = \theta_2 < \theta_1$, $\gamma = \frac{7}{5}$, $M_0 = 1{\cdot}60$, $\theta'_w = 42{\cdot}12°$, $M_s = 1{\cdot}18$. (*b*) $\theta_3 = \theta_2 > \theta_1$, $\gamma = \frac{7}{5}$, $M_0 = 1{\cdot}50$, $\theta'_w = 40{\cdot}33°$, $M_s = 1{\cdot}14$.

criteria based on M_{2T} for the existence of SMR, CMR and DMR in diatomic gases. SMR occurs if

$$M_{2T} < 1. \tag{6}$$

A CMR takes place when

$$1 < M_{2T} < 1{\cdot}3. \tag{7}$$

A DMR results for all

$$M_{2T} > 1{\cdot}3. \tag{8}$$

The gasdynamic reasons for the transitions SMR → CMR (when the flow behind the reflected shock wave becomes supersonic with respect to the first triple point) and CMR → DMR (when this flow becomes supersonic with respect to the kink) suggests that if the flow behind M_1 (figure 1*d*) becomes supersonic with respect to the second triple point T_1 ($M_{5T_1} > 1$) a new second kink will occur. If this flow now becomes supersonic with respect to the second kink a triple-Mach reflexion (TMR) could form. In order to verify these hypotheses, reflexions must be obtained using very strong incident shock waves as well as long compression models in order to allow the shock wave configuration to develop to a significant size. Unfortunately, experiments with high Mach numbers ($M_s > 8$) involve the risk of damaging the interferometric optical windows of the test section of the shock tube used for the present study. Consequently, it was not possible to verify the existence of TMR in the present study.

Additional flow properties from (P, θ) *polars.* It has been found that the I and R polars can take on two basically different combinations immediately after RR

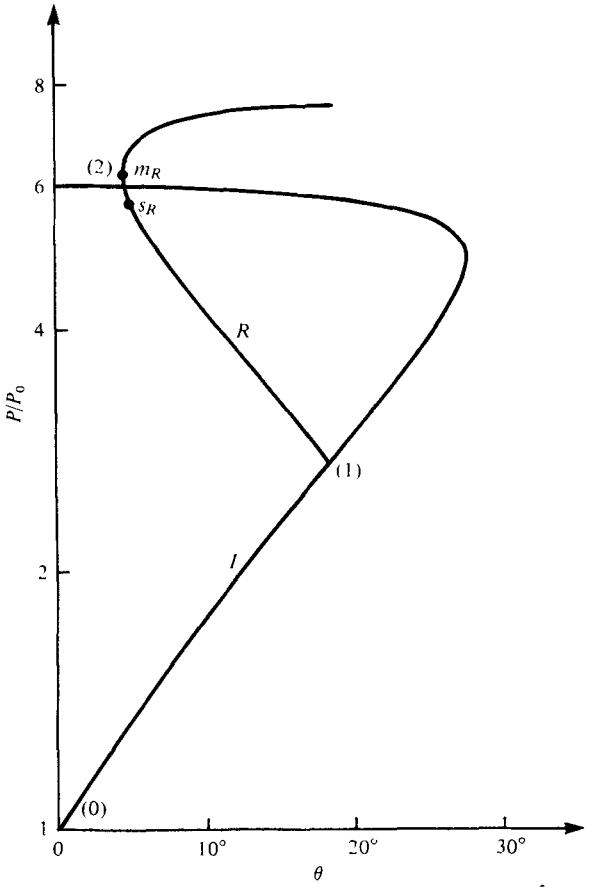

FIGURE 9. I and R polar combination for $2{\cdot}19 < M_0 < 2{\cdot}40$, $\gamma = \frac{7}{5}$, $M_0 = 2{\cdot}30$, $\theta'_w = 46{\cdot}27°$, $M_s = 1{\cdot}59$.

termination. In one of them, the solution in the (P, θ) plane (figure 8a) indicates that the flow is redeflected by R so that $\theta_3 = \theta_2 < \theta_1$, while the other (figure 8b) gives $\theta_3 = \theta_2 > \theta_1$ and the flow is further deflected by R. A limiting condition between these two cases exists when $\theta_3 = \theta_2 = \theta_1$, and there is no deflexion through R (in the vicinity of the triple point T), i.e. R is normal to the streamlines. Note that for $M_0 < M_{0_c}$ the termination of RR will always result in a SMR, since the solution in the (P, θ) plane always lies on the strong portion of the R polar and hence $M_{2T} < 1$ (figures 8a, b).

For $M_0 > M_{0c}$ where the point of tangency between the R polar and the P axis lies outside the I polar (figure 2a, R_{iv} state 2′ or f) M_{2T} will be less than unity (immediately after RR termination) in a small range where the intersection of the I and R polars lies between the sonic point s_R and the point of maximum deflexion m_R on the R polar (figure 9). For higher values of M_0, the termination of RR will result in $M_{2T} > 1$ and hence a SMR is not possible. However, any value of M_0 can be matched with a corresponding value of ϕ_0 ($\phi_0 = 90° - \theta'_w$) for which, again, $M_{2T} \leqslant 1$ (figure 10, R_{iii}).

When the intersection point on the R polar lies below the sonic point (figure 10, R_{i}) a SMR is not possible, since the supersonic flow (behind R) $M_{2T} > 1$ moves toward the wedge surface $\theta_2 \neq 0$. Physically, this flow must either turn away from the surface

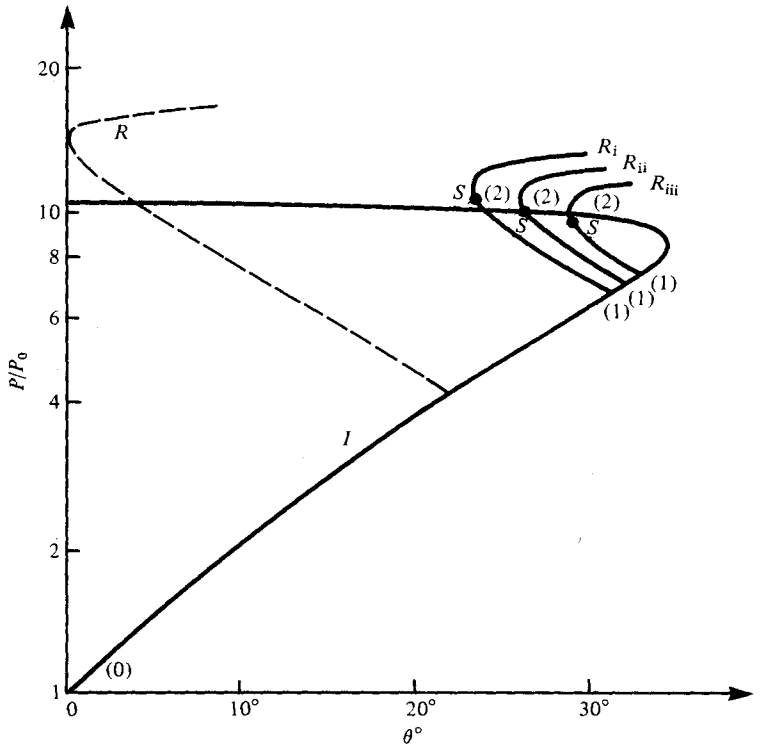

FIGURE 10. Three consecutive combinations of I and R polars illustrate transition from complex (CMR) to single (SMR) Mach reflexion. Nitrogen, $P_0 = 15$ torr, $T_0 = 300$ K, $M_0 = 3{\cdot}00$. (i) $M_{2T} > 1$, CMR ($\theta'_w = 36{\cdot}02°$, $M_s = 2{\cdot}43$). (ii) $M_{2T} = 1$, termination of CMR and formation of SMR ($\theta'_w = 34{\cdot}07°$, $M_s = 2{\cdot}49$). (iii) $M_{2T} < 1$, SMR ($\theta'_w = 32{\cdot}10°$, $M_s = 2{\cdot}54$).

or change into a subsonic flow by passing through a shock wave in order to negotiate the surface. In practice when the flow behind the reflected shock becomes supersonic with respect to the first triple point ($M_{2T} > 1$) a kink forms in the reflected shock wave and SMR terminates to form a CMR.

Henderson & Lozzi (1975) advanced the hypothesis that this kink is probably caused by a 'band of compression' which turns the supersonic flow away from the wall. We have verified their hypothesis experimentally from a plot of isopycnics in CMR. They show convergence as a compression wave on the reflected shock waves (see subsequent figures 15*d*, *e*). Consequently, a kink forms in the reflected wave at this convergence. For even higher values of M_s, the compression wave converges to form a shock wave, which results in a DMR configuration.

Reflexions in the (M_s, θ'_w) *plane.* It is worth re-examining figure 6 in the light of the above criteria for the formation and termination of RR, SMR, CMR, DMR and NR in the (M_s, θ'_w) plane. The dashed lines are for a perfect gas ($\gamma = \frac{7}{5}$), while the solid lines account for real-gas effects in nitrogen with four (numbered 1–4) different initial pressures $P_0 = 1$, 10, 100 and 1000 torr, respectively. It can be seen that the real-gas boundaries start to drop from their perfect-gas values at very low incident shock wave Mach numbers M_s due to the temperature-dependent vibrational excitation. At higher values of M_s each boundary line splits and falls even further with decreasing initial pressure as a result of dissociation. At still higher shock Mach

numbers electronic excitation and ionization would play similar roles. Under such conditions the sharp boundary lines which exist for a perfect gas between the domains of the different types of reflexion are replaced by a multiplicity of lines depending on the initial pressure and temperature. For example one would expect a RR for $M_s = 10$ and $\theta'_w = 45°$ when the initial pressure $P_0 > 1000$ torr and a DMR when $P_0 < 100$ torr ($\theta_1 + \theta_{2m} = 0$, lines 4 and 2, respectively). As M_s approaches unity, the line for $\theta_1 + \theta_{2m} = 0$ approaches the line for $M_1 = 1{\cdot}00$. These two lines are coincident at the origin ($M_s = 1, \theta'_w = 0$). Consequently, RR can be obtained with very low wedge angles providing the incident shock wave is sufficiently weak. Note that White (1951) reported RR with $\theta_w = 22°$ and $M_s = 1{\cdot}022$; $\theta_w = 30°$ and $M_s = 1{\cdot}018$; $\theta_w = 38°$ and $M_s = 1{\cdot}065$.

It can be seen from figure 6 that in non-stationary flows all transitions from RR to SMR, CMR, DMR can occur over a very small range of Mach numbers (points *a*–*b*). Alternatively, if M_s is fixed transitions from RR to SMR, to (CMR, SMR) or to (DMR, CMR, SMR) can be made by decreasing θ'_w (or θ_w). This figure finally clears up some of the disagreements between various investigators who reported different sequences of events as one passed through a range of wedge angles θ_w for a fixed M_s. They were unaware of the domains and their transition boundaries presented in figure 6. The different sequences of events (and experimental investigations) are summarized as follows: $1{\cdot}00 < M_s < 1{\cdot}60$ (point *a*), RR → SMR (Bleakney & Taub 1949); $1{\cdot}60 < M_s < 2{\cdot}69$ (point *b*), RR → CMR → SMR (Smith 1945); and $M_s > 2{\cdot}69$, RR → DMR → CMR → SMR (Kutler & Shankar 1977; Shankar *et al.* 1977).

Alternatively, if one starts with a fixed wedge angle and increases the incident shock wave Mach number, the following transitions will be encountered. At very low Mach numbers a RR will result (e.g. $\theta'_w = 40°$). As M_s increases the detachment criterion will be exceeded and RR will terminate to form a SMR where the flow behind the reflected shock wave is subsonic ($M_{2T} < 1$) with respect to the triple point. When M_s increases, M_{2T} increases until it becomes supersonic with respect to T, a kink develops in the reflected shock wave and the transition SMR → CMR occurs. At this stage the flow behind the reflected shock wave is subsonic with respect to the kink ($M_{2K} < 1$). However, upon a further increase in M_s, this flow becomes supersonic with respect to the kink and the transition CMR → DMR takes place.

It should be stressed that all the lines in figure 6 were obtained analytically. The lines $M_{2T} = 1{\cdot}00$ and $M_{2K} = 1{\cdot}00$ were found by solving the 14 nonlinear oblique shock-wave equations (with 14 unknowns) that describe the three-shock confluence at a triple point and transforming the dynamic properties of state (2) behind the reflected shock wave R, from a frame of reference attached to the first triple point T to a frame of reference attached to the kink K. The line $\theta_1 + \theta_{2m} = 0$ was determined by solving the 9 nonlinear oblique shock-wave equations (with 9 unknowns) that describe RR. To the best of our knowledge this is the first time that these two sets of nonlinear equations were solved for real gases (Ben-Dor 1978*a*). Henderson (1964) solved these two sets for perfect gases. The line $M_1 = 1{\cdot}00$ was obtained by solving the 4 nonlinear equations (with 4 unknowns) that describe the flow through an oblique shock wave (see Ben-Dor (1978*a*) for further details).

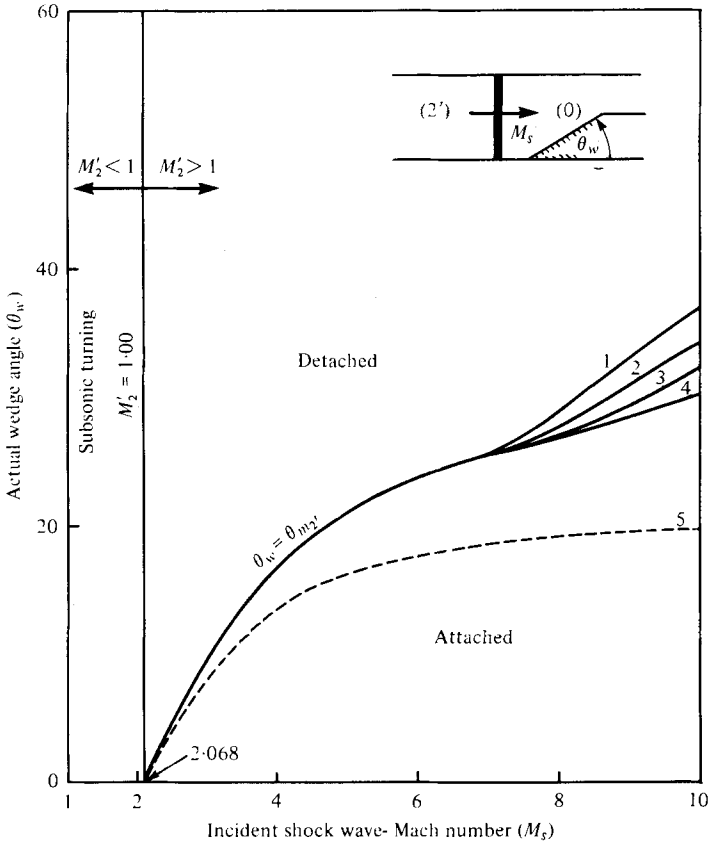

FIGURE 11. Deflexion processes of the shock-induced quasi-steady flow (2′) as a function of M_s and θ_w. Lines (1)–(4) are for imperfect nitrogen $T_0 = 300$ K and $P_0 = 1$, 10, 100 and 1000 torr, respectively. Line 5 is for a perfect gas $\gamma = \frac{7}{5}$.

2.2. *Induced-flow deflexion*

It was noted previously that oblique shock-wave diffractions in non-stationary flows also depend on the flow-deflexion process over the corner. Consider a planar shock wave propagating in a shock tube (figure 11) and denote the state behind it as (2′). For any given initial conditions (P_0, T_0) and incident shock wave Mach number M_s, the induced flow Mach number $M_{2'}$ as well as $P_{2'}$ and $T_{2'}$ can be calculated. Consequently, the corresponding sonic deflexion angle $\theta_{s2'}$ and the detachment angle $\theta_{m2'}$ can be determined. Therefore, the (M_s, θ_w) plane can be divided into two main regions, one corresponds to $M_{2'} < 1$, where the flow turns the corner subsonically, and the other to $M_{2'} > 1$, where the turn takes place through a bow wave. The latter can be subdivided into three different flow-deflexion regions: $0 < \theta_w < \theta_{s2'}$ for a deflexion through a straight and attached oblique shock wave; $\theta_{s2'} < \theta_m < \theta_{m2'}$ for a deflexion through a curved (but straight at the very leading edge) and attached shock wave; $\theta_w > \theta_{m2'}$ where the deflexion is through a curved detached shock wave. Since the maximum separation between $\theta_{m2'}$ and $\theta_{s2'}$ for real nitrogen ($P_0 = 15$ torr, $T_0 = 300$ K) was found to be 0·63° only two regions $0 < \theta_w < \theta_{m2'}$ and $\theta_w > \theta_{m2'}$ need be considered for practical purposes.

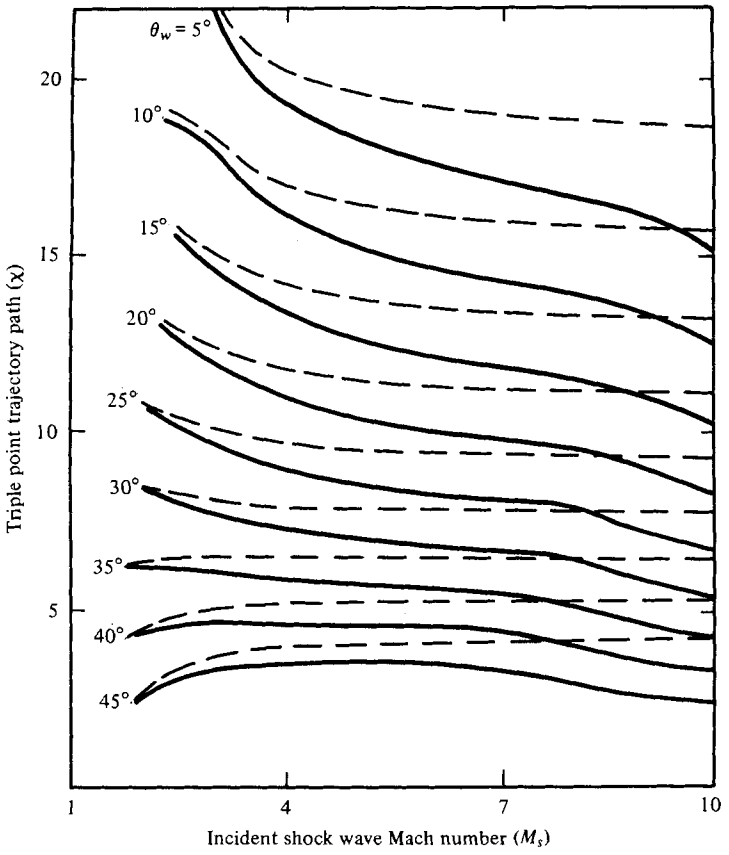

FIGURE 12. Variation of the triple-point trajectory angle χ with incident shock Mach number M_s for given wedge angles θ_w. ——, imperfect nitrogen, $P_0 = 15$ torr, $T_0 = 300$ K; – – –, perfect gas $\gamma = \frac{7}{5}$.

The deflexion processes in the (M_s, θ_w) plane are shown in figure 11. The dashed line is for a perfect gas ($\gamma = \frac{7}{5}$), while the solid lines are for real nitrogen with four (1–4) different initial pressures $P_0 = 1$, 10, 100 and 1000 torr, respectively, at a temperature of 300 K. One should also note that the line $M_2 = 1$ corresponds to $M_s = 2{\cdot}068$ (for a perfect gas) and to 2·055 with vibrational excitation. The difference between these two lines cannot be plotted on figure 11. The deflexion process depends strongly on initial pressure for a given initial temperature. For $M_s = 10$ and $\theta_w = 35°$ the flow will negotiate the corner through an attached shock wave if $P_0 = 1$ torr or less and through a detached shock wave if $P_0 = 10$ torr or more.

2.3. *Oblique shock-wave-diffraction regimes*

Figures 6 and 11, which correspond to non-stationary shock-wave-reflexion and flow-deflexion processes, respectively, can be superimposed to obtain the overall shock-wave-diffraction phenomena. However, note that their vertical axes are different. In figure 6, θ_w' equals θ_w in the RR regime and $\theta_w + \chi$ elsewhere. Consequently, χ must be subtracted prior to any superposition. To do so, we have made use of the best available analytical approach to date for obtaining $\chi(M_s, \theta_w)$ developed by Law

& Glass (1971). A plot of χ *vs.* M_s and θ_w for nitrogen at $P_0 = 15$ torr, $T_0 = 300$ K and a perfect gas with $\gamma = \frac{7}{5}$ (dashed) is shown in figure 12. It is seen that χ is in general a decreasing function with increasing θ_w and M_s. However, its dependence on M_s is stronger for small wedge angles θ_w, e.g. when M_s increases from 2·5 to 10, χ changes gradually from 18 to 13° for $\theta_w = 10°$, while for $\theta_w = 40°$ it varies only from 4 to 2·5°. Note that the perfect-gas lines level out as M_s increases, resulting in χ being independent of M_s or $\chi = \chi(\theta_w)$.

The interaction between the shock-wave-reflexion phenomenon and the induced flow-deflexion process causes the reflected shock wave R to curl back towards the model and terminate at the wedge corner or the shock-tube wall. Since the shock-wave configuration is growing with time, the point where R terminates at the shock-tube wall moves towards the oncoming shock-induced flow. Consequently, the relative induced flow Mach number with respect to the perpendicular part of the reflected shock wave near the wall is increased. Therefore, the subsonic turning region shown in figure 11 cannot become established in non-stationary flows. For incident shock waves in the range $1 < M_s < 2{\cdot}068$ the reflected shock wave R is continuously weakening as one moves along it away from the triple point. For very weak incident shock waves (see subsequent discussion and figures 17*a*, *b*) R degenerates to a Mach wave by the time it reaches the wall. At the limiting case of a degenerated incident shock wave ($M_s = 1$), the reflected shock wave becomes a Mach wave over its entire length (Bargmann 1945). Therefore, as there are four reflexion processes (RR, SMR, CMR, DMR) and two deflexion processes (an attached or a detached shock wave), a maximum of eight different shock-wave diffraction systems are possible.

Figure 6 (with χ subtracted) and figure 11 were superimposed to obtain figure 13 (only the boundary lines corresponding to $P_0 = 15$ torr are reproduced). Out of the maximum of eight possible shock-wave diffractions only seven are obtained in the range $1 \leqslant M_s \leqslant 10$. The unobtainable diffraction is a RR with an attached shock wave at the wedge corner. Note that if the line $\theta_1 + \theta_{2m} = 0$ and the attached/detached line are extrapolated beyond $M_s = 10$ they might intersect, and hence a RR with an attached shock wave could be obtained. These two lines could also intersect in the range $1 \leqslant M_s \leqslant 10$ by decreasing the initial pressure P_0. Note from figures 6 and 11 that as P_0 decreases these two lines approach. However, care must be taken that P_0 is not reduced to a value where the continuum assumption is violated. The seven different shock-wave diffractions in the range $1 \leqslant M_s \leqslant 10$ are listed in table 1. They consist of a RR with a detached shock wave (region 1), SMR having a detached or an attached shock wave (regions 2 and 3, respectively), CMR with deflexion through a detached or an attached shock wave (regions 4 and 5 respectively), and finally DMR with a detached (region 6) or an attached (region 7) shock wave.

The experimental fact that the incident shock wave reflects even from very small wedge angles (note that we could not go below $\theta_w = 2°$ due to the physical limitations of machining) led us to the conclusion that shock-wave reflexions always occur (i.e. even in the range $0 \leqslant \theta_w \leqslant 2°$). Therefore, the boundary line for no reflexion NR in figure 6 ($M_1 = 1{\cdot}00$) was omitted from figure 13, i.e. it is assumed that on the line $M_1 = 1{\cdot}00$ (figure 6) $\theta'_w = \chi$. Since $\theta'_w = \theta_w + \chi$ by definition, the transformation from θ'_w to θ_w yields that the line $M_1 = 1{\cdot}00$ in figure 6 coincides with the line $\theta_w = 0$ in figure 13. Consequently, in non-stationary flows the NR region does not exist.

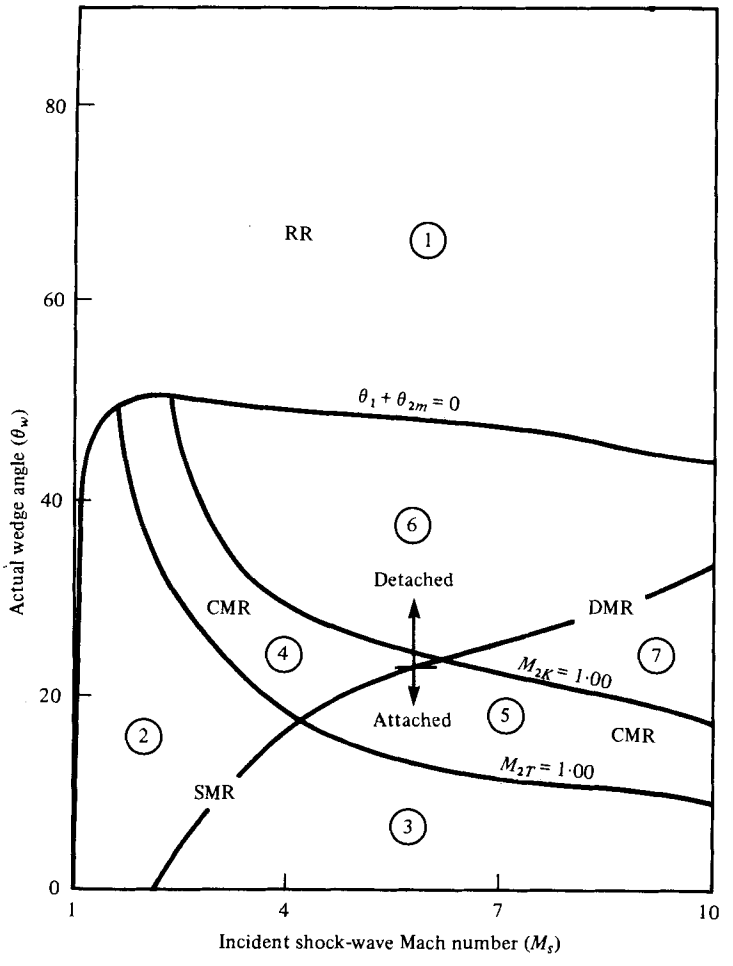

FIGURE 13. Seven domains and their transition boundaries of shock-wave diffractions in non-stationary flows in (M_s, θ_w) plane resulting from present analysis (see table 1).

	Shock diffraction	
Region no.	Shock reflexion	Flow deflexion
1	RR	Detached
2	SMR	Detached
3	SMR	Attached
4	CMR	Detached
5	CMR	Attached
6	DMR	Detached
7	DMR	Attached

TABLE 1. Diffraction regions in figures 13 and 20.

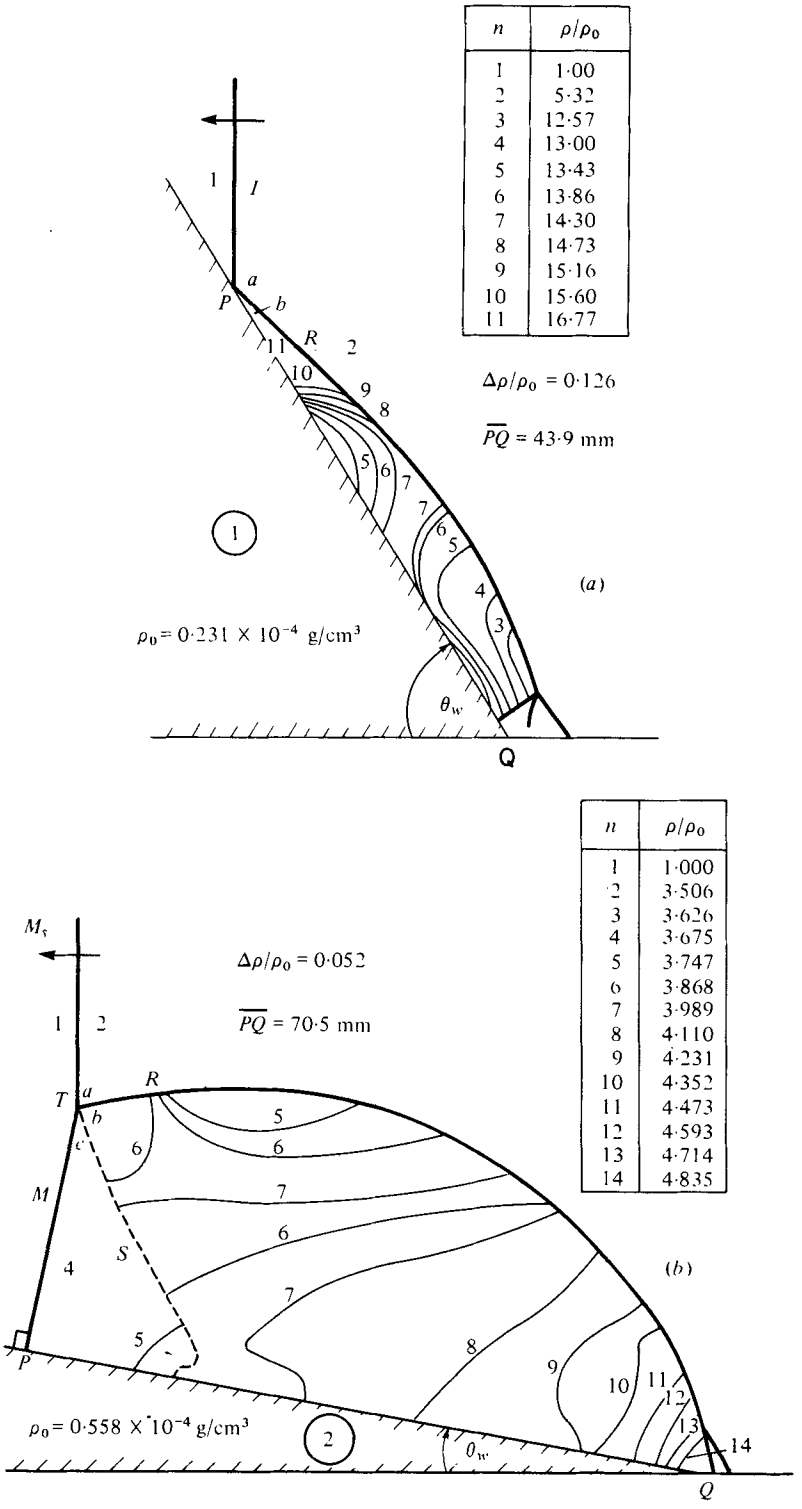

FIGURE 15 (*a*, *b*). For legend see p. 484.

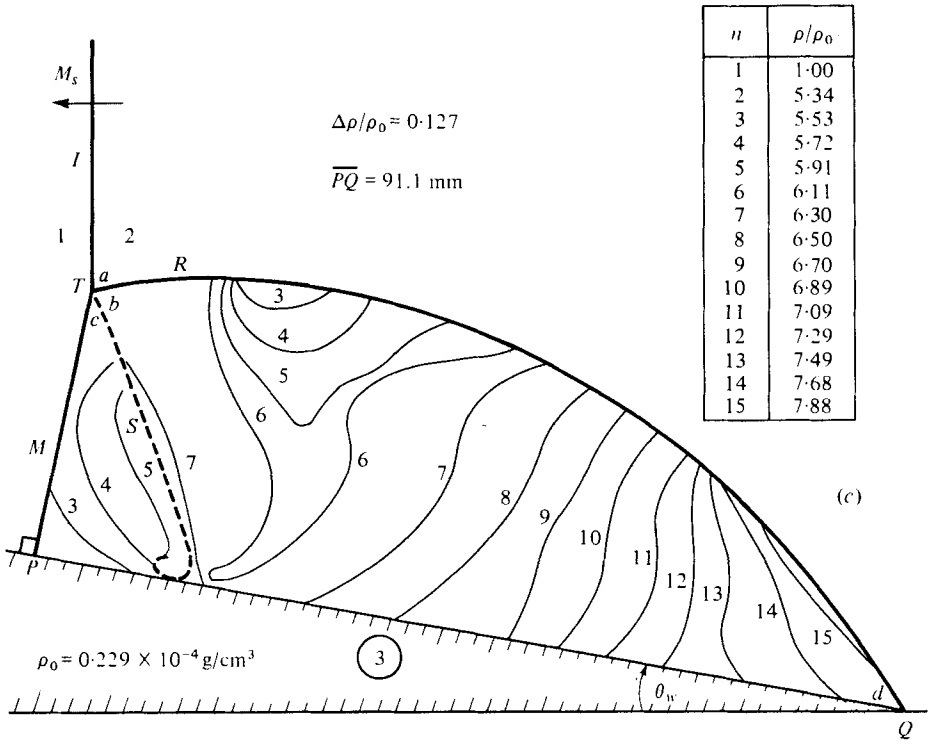

n	ρ/ρ_0
1	1·00
2	5·34
3	5·53
4	5·72
5	5·91
6	6·11
7	6·30
8	6·50
9	6·70
10	6·89
11	7·09
12	7·29
13	7·49
14	7·68
15	7·88

n	ρ/ρ_0
1	1·000
2	4·780
3	6·013
4	6·230
5	6·447
6	6·663
7	6·880
8	7·097
9	7·314
10	7·530
11	7·747
12	7·963
13	8·180
14	8·397
15	8·613
16	8·830

FIGURE 15 (*c*, *d*). For legend see p. 484.

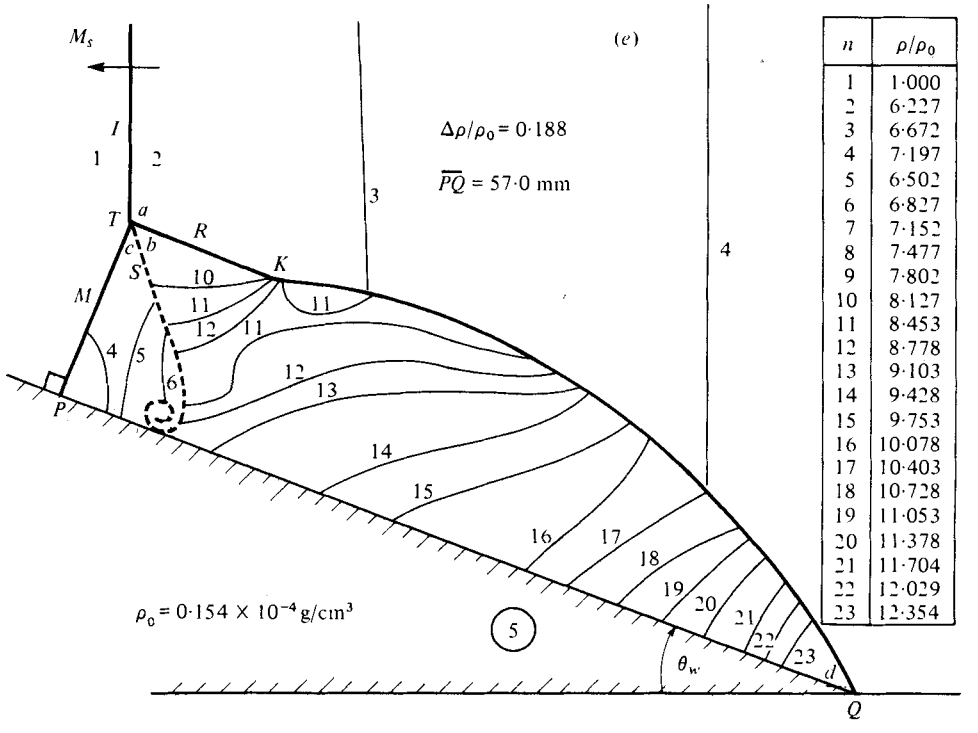

n	ρ/ρ_0
1	1·000
2	6·227
3	6·672
4	7·197
5	6·502
6	6·827
7	7·152
8	7·477
9	7·802
10	8·127
11	8·453
12	8·778
13	9·103
14	9·428
15	9·753
16	10·078
17	10·403
18	10·728
19	11·053
20	11·378
21	11·704
22	12·029
23	12·354

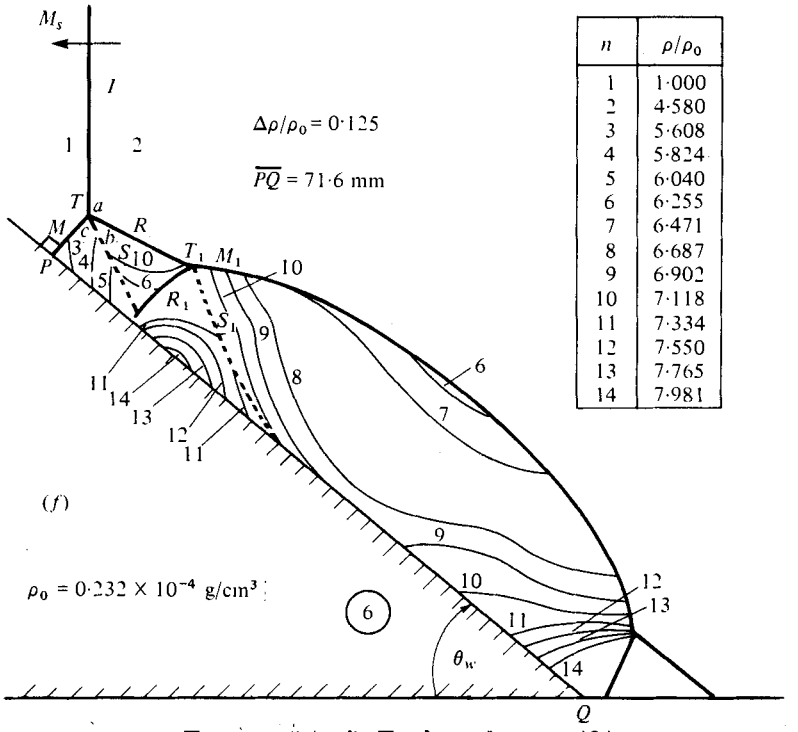

n	ρ/ρ_0
1	1·000
2	4·580
3	5·608
4	5·824
5	6·040
6	6·255
7	6·471
8	6·687
9	6·902
10	7·118
11	7·334
12	7·550
13	7·765
14	7·981

FIGURE 15 (*e*, *f*). For legend see p. 484.

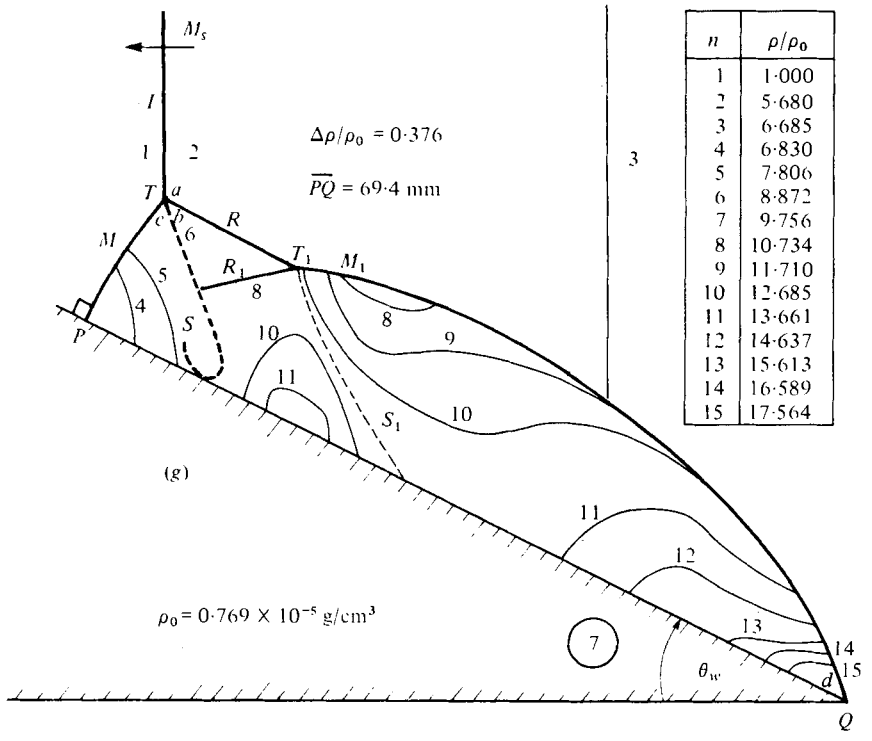

n	ρ/ρ_0
1	1·000
2	5·680
3	6·685
4	6·830
5	7·806
6	8·872
7	9·756
8	10·734
9	11·710
10	12·685
11	13·661
12	14·637
13	15·613
14	16·589
15	17·564

FIGURE 15. Actual flow isopycnics corresponding to the seven interferograms of the seven different oblique shock-wave diffractions shown in figure 14 (with identical initial conditions). Calculated densities (ρ/ρ_0) are: (*a*) *a*, 5·32; *b*, 17·66 (4·88, 14·48). (*b*) *a*, 3·550; *b*, 3·855; *c*, 3·705 (3·505, 3·806, 3·678). (*c*) *a*, 5·34; *b*, 6·11; *c*, 5·59 (4·90, 5·47, 5·03). (*d*) *a*, 4·580; *b*, 6·489; *c*, 5·282 (4·376, 6·066, 4·861). (*e*) *a*, 7·191; *b*, 9·131; *c*, 7·570 (6·148, 7·585, 6·300). (*f*) *a*, 4·586; *b*, 7·908; *c*, 5·669 (4·383, 7·286, 5·086). (*g*) *a*, 6·685; *b*, 9·184; *c*, 7·347 (5·566, 7·339, 5·699). The imperfect values are given for the location *a*, *b* or *c* at the vicinity of the triple point or reflexion point. The values in brackets are the respective values for a perfect gas.

2.4. *Density fields for the various diffractions*

The seven shock-wave diffraction domains corresponding to regions 1–7 of figure 13 are shown in the interferograms, figure 14(*a*)–(*g*), respectively (plates 2–5). The density distributions (ρ/ρ_0) in the flow fields, in the form of isopycnics (n) associated with each diffraction process are shown in figures 15(*a*)–(*g*). The density profiles along the wedge and the shock-tube wall appear in figures 16(*a*)–(*g*). A general description is given of each diffraction as well as their similarities and differences.

In figures 16(*a*, *b*, *d*, *f*) which correspond to flow deflexion through detached shock waves (regions 1, 2, 4 and 6 of figure 13), shock-wave bifurcation and boundary-layer roll-up are clearly seen (for further details see Ben-Dor 1978*a*). As mentioned earlier, when the Mach number of the incident shock wave decreases, the strength of the reflected shock wave decreases. Consequently, at low values of M_s the bifurcation process does not occur. White (1951) in his pioneering work was able to produce some very weak incident shock waves. Figures 17 (*a*, *b*) are reproductions of two of his figures. The initial conditions for these two pictures are $M_s = 1{\cdot}010$, $\theta_w = 5{\cdot}7°$ (SMR) and $M_s = 1{\cdot}018$, $\theta_w = 30°$ (RR), respectively. For these low values of M_s the reflected shock wave degenerates to a Mach wave (the weakest possible detached shock wave)

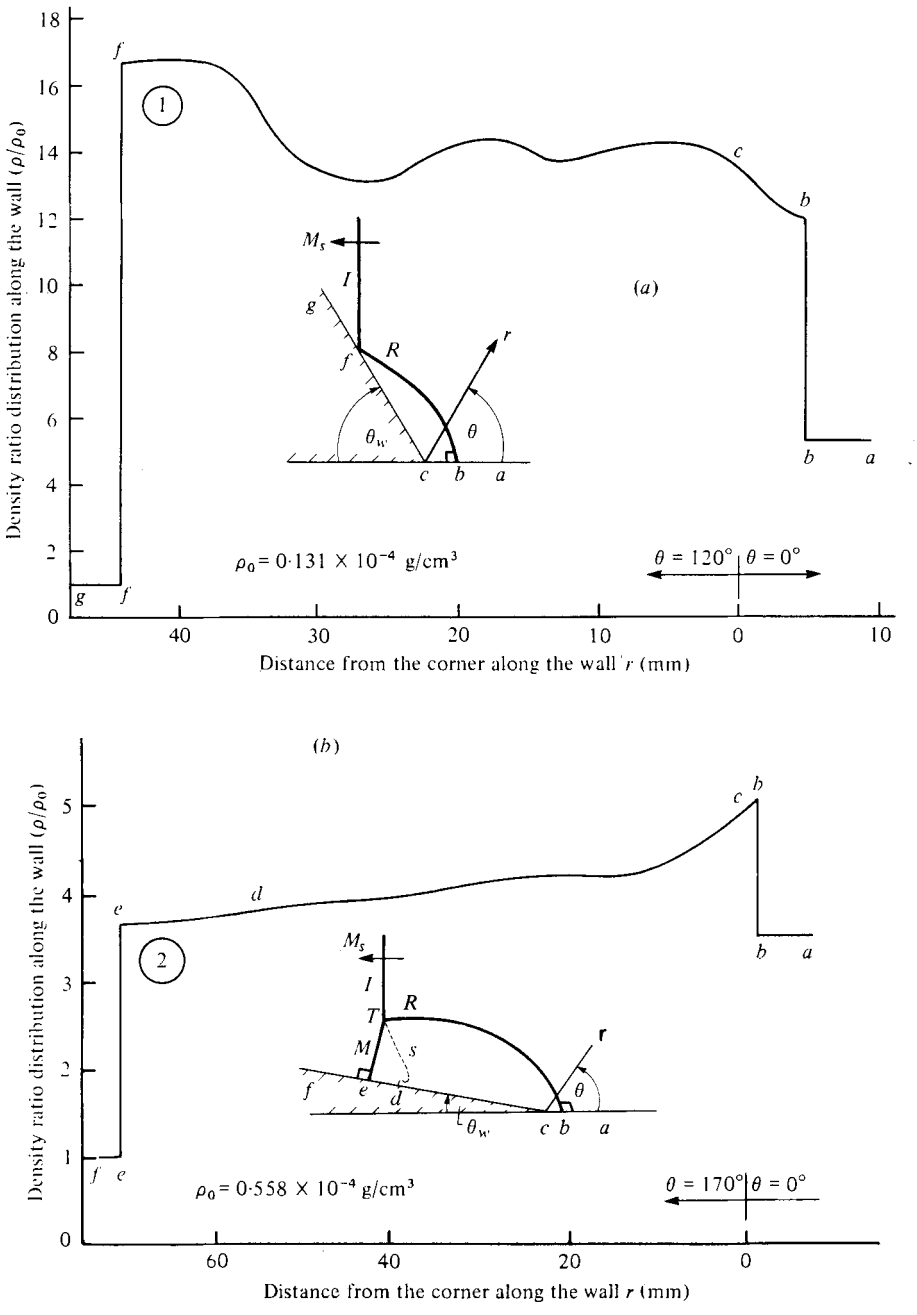

FIGURE 16 (*a*, *b*). For legend see p. 488.

and the shock-induced flow turns over the wedge subsonically. Note that for these two examples from White (1951) the induced flow Mach number M_2 is 0·017 and 0·029, respectively.

Since the flow deflexion over the corner is achieved through an attached or detached shock wave there is a sharp density jump at the point *b*. In the case of an attached shock wave at the corner (figures 14*c*, *e*, *g*) the highest density along the wall is measured

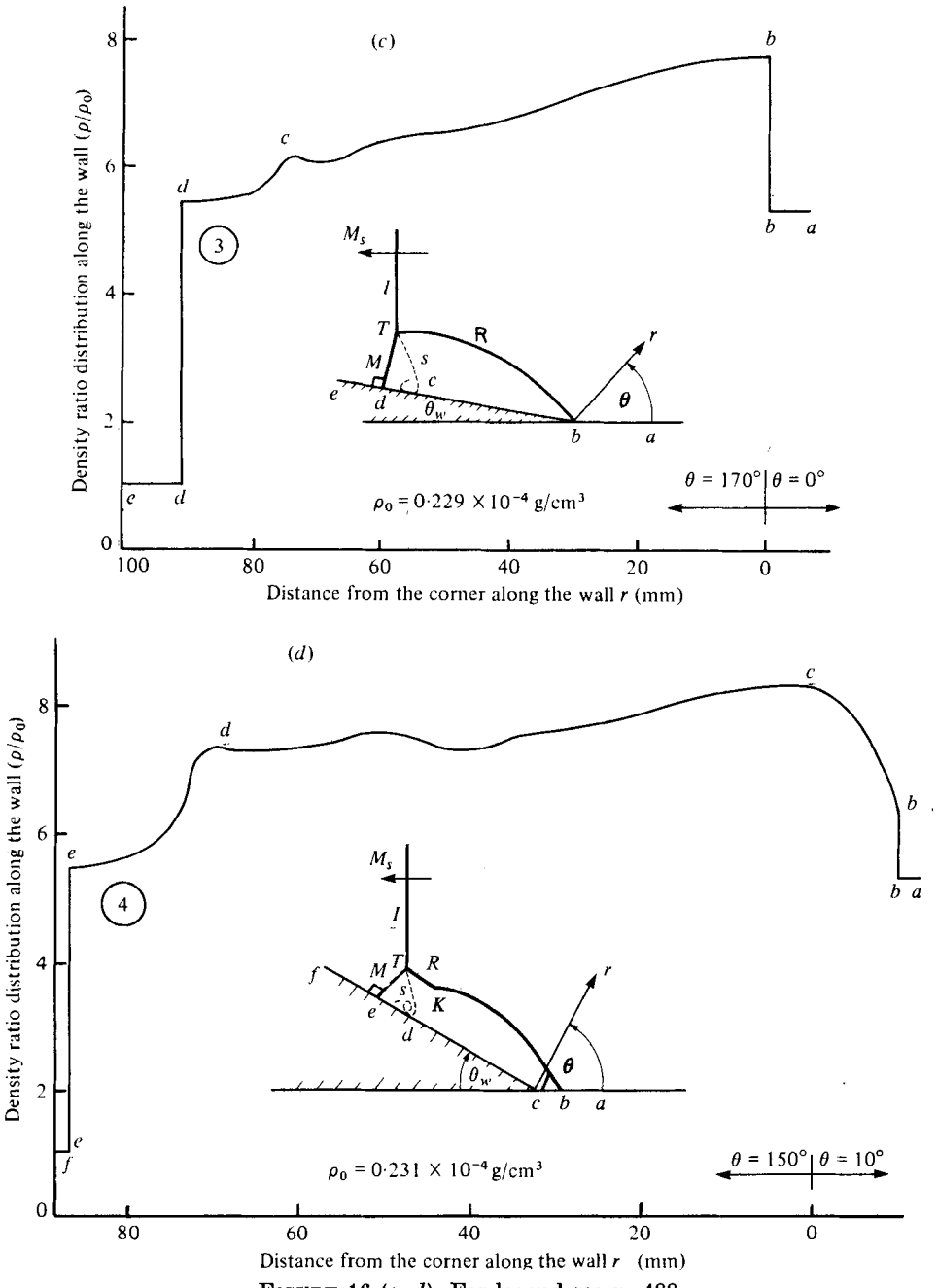

FIGURE 16 (*c*, *d*). For legend see p. 488.

immediately behind the attached shock wave, i.e. at the corner point *b*, figures 16*c*, *e*, *g*) while in the case of a detached shock wave (figures 14*a*, *b*, *d*, *f*) the highest density may or may not be (figures 16*a*, *d*) behind this shock wave or at the corner.

The existence of a compression wave at the kink *K* of a CMR can be clearly seen in figures 15(*d*, *e*), where the isopycnics converge. The corresponding compression strengths (density ratios) are approximately: 6·880/6·447 and 8·778/8·127 or 1·067

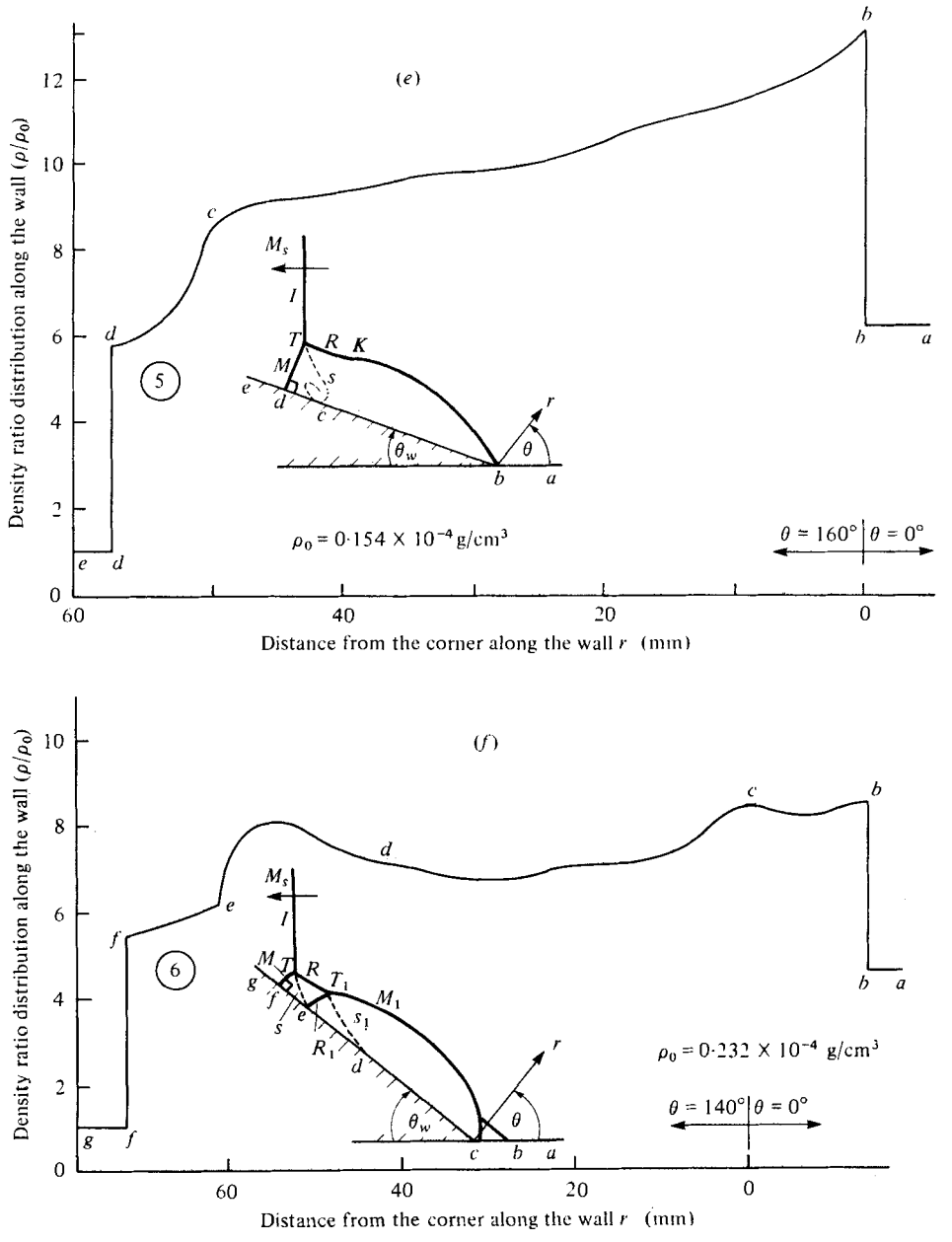

FIGURE 16 (*e*, *f*). For legend see p. 488.

and 1·080, respectively. For compressions of 1·067, 1·080 an increasingly clearer kink can be seen (figures 14*d*, *e*). The equivalent perfect shock wave Mach numbers that would give the same compressions are 1·040 and 1·048. The calculated flow Mach numbers behind the reflected wave M_{2T} in the vicinity of the triple point T are 1·251 and 1·301, respectively. Once a DMR is formed ($M_{2K} > 1{\cdot}00$) the isopycnics do not converge any more (figures 15*f*, *g*) and the compression wave is replaced by a shock wave.

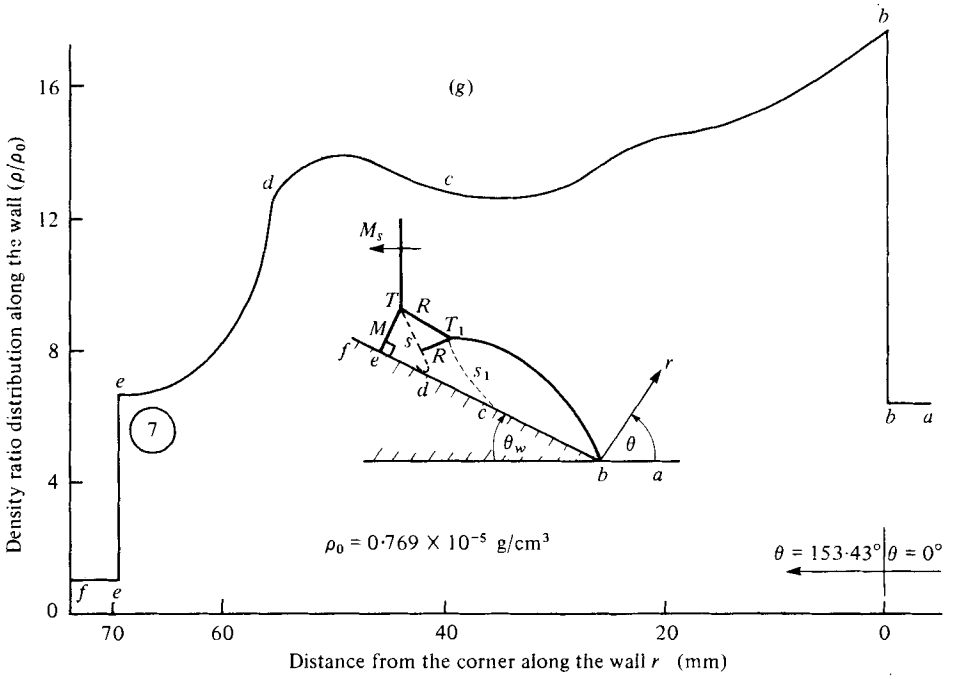

FIGURE 16. Interferometric density-ratio distributions along the wall for seven different oblique shock-wave diffractions shown in figure 14 (with identical initial conditions).

In the cases of SMR (figures 15*b*, *c*) the convergence of the isopycnics corresponds to a weak-expansion wave rather than a compression wave (follow the isopycnic numbers). The strengths of these expansion waves are: 3·747/3·868 and 5·53/6·11 or 0·969 and 0·905, respectively. The case with an attached shock wave has the stronger expansion. This is also true for CMR, where the case with an attached shock wave has the stronger compression (figures 15*e*). Figures 16(*b*)–(*g*) show that the density along the wedge surface always increases as one moves from the Mach stem towards the point where the slipstream disappears into the boundary layer. Consequently the flow behind the Mach stem is being further compressed.

Although the density flow fields associated with the various shock-wave diffractions differ greatly, nevertheless, they do have some similarities. For example, in the case of an attached shock wave (figures 15*c* SMR and *e* CMR), the isopycnics tend to run perpendicular to the reflected shock wave. In the case of DMR (figures 15*f*, *g*) a 'corridor' is formed for the second slipstream. In figure 14(*g*) the second slipstream is not visible. The change in density is not sufficiently large to establish a noticeable fringe shift. Therefore, a thin dashed line has been drawn to indicate the possible location of the second slipstream in figure 15(*g*).

The density at any point (x, y) can be calculated either by interpolating between or extrapolating beyond the isopycnic in the vicinity of that point. However, since the density difference between the isopycnics is quite small, any region between them can be assumed to have a uniform average value. For a region where the density change was not sufficiently large to plot isopycnics it can be assumed to be uniform with the indicated density number. For example, region $n = 6$ bounded by R, R_1 and

n	ρ/ρ_0
1	1·000
2	1·015
3	1·079
4	1·070
5	1·061
6	1·052
7	1·043

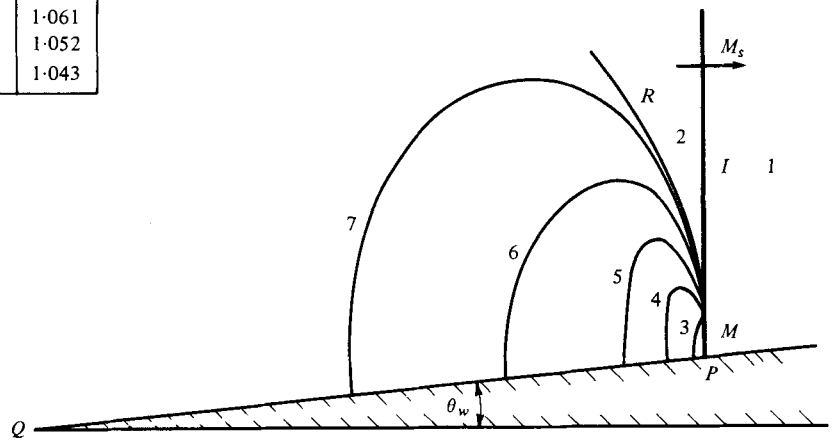

n	ρ/ρ_0
1	1·000
2	1·029
3	1·057
4	1·054
5	1·050
6	1·046
7	1·043
8	1·039
9	1·035

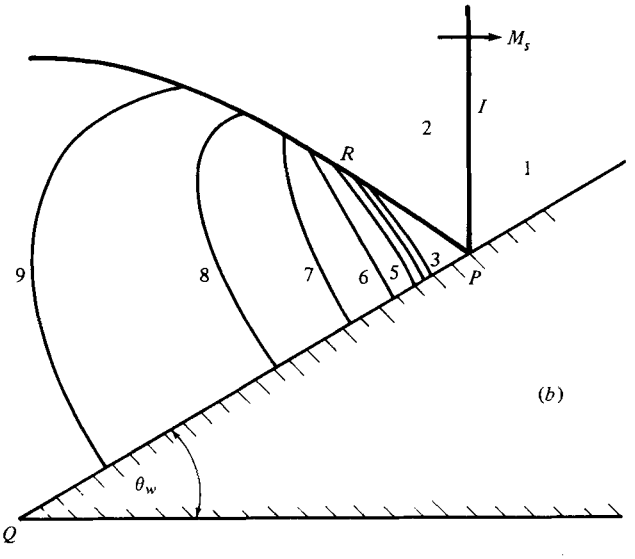

FIGURE 17. Shock-wave diffractions in air with degenerated reflected shock waves, R. Reproduction of figures 34 and 46 from White (1951): (*a*) SMR, $M_s = 1{\cdot}010$, $\theta_w = 5{\cdot}7°$; (*b*) RR, $M_s = 1{\cdot}018$, $\theta_w = 30°$.

S in figure 15 (g) is uniform with $\rho = 8{\cdot}87\rho_0$. The relative error in the measured density is given in every figure by $\Delta\rho/\rho_0$ and is fixed for that particular experiment. It can be as high as 37·6 % for ρ_0 corresponding to $P_0 = 5$ torr (figure 15g), and as low as 5·2 % for a ρ_0 corresponding to $P_0 = 37$ torr (figure 15b). However, this is a severe test and it would have been better to refer to $\Delta\rho/\rho_2$ or $\Delta\rho/\rho_3$, since ρ_2 and ρ_3 are well known, thereby reducing the relative error by several factors. Each fringe could be measured to an accuracy of 0·05–0·1 of a fringe. The position in the (x, y) plane of a point on any isopycnic is known to $\pm$ 1 mm. Our data forms a very accurate and comprehensive base for comparison with inviscid numerical analyses (Ben-Dor & Glass 1978), as the refraction errors due to wall boundary layers are negligible. The same methods were used for ionizing shock structure and boundary layers (Glass & Liu 1978; Liu, Whitten & Glass 1978). In these problems with very large density gradients where refraction errors might have been more significant, they were also found to be negligible and very good agreement was obtained between sophisticated numerical analyses and experiments. Consequently, the interferometric isopycnics of the flow can be used now and in the future as a check in the development of computational methods for non-stationary oblique shock-wave reflexions.

3. Verification of diffraction domains and boundaries

The major task was to show that our analysis predicting the seven regions and their transition boundaries in non-stationary oblique shock wave reflexion was verified by experiment. If so, it would bring understanding and order into an area that has been researched for over three decades. For this purpose 58 successful experiments were done in the 10 × 18 cm UTIAS Hypervelocity Shock Tube. A 23 cm diameter Mach–Zehnder interferometer was used for recording the non-stationary process. The light source consisted of a giant-pulse ruby laser. Simultaneous dual-frequency interferograms were taken at wavelengths of 6943 and 3471·5 Å. Wedges with $\theta_w = 2$, 5, 10, 20, 26·56, 30, 40, 50 and 60° ($\pm$ 0·0167°) were used. Each wedge was fastened to the lower wall of the test section of the shock tube. The clearance between the wedge and the shock-tube side walls or windows was 0·025 mm. Although this arrangement tends to introduce boundary-layer interaction at the wedge corner, it was adopted owing to the simplicity in design and rigid fastening which is especially important on impact with a strong shock wave. For each wedge angle θ_w, about six experiments were made at the following nominal incident shock-wave Mach numbers $M_s = 2{\cdot}0$, 3·7, 4·7, 6·0, 7·0, 8·0. Over this range the Mach number varied by about 0·1. Note that some of the experiments were repeated in order to check and ensure repeatability. The accuracy in measuring the shock-wave Mach number was

$$dM_s = 0{\cdot}0015M_s^2 + 0{\cdot}0102M_s,$$

which gives a relative error of 1·00 % at $M_s = 2{\cdot}0$ ($dM_s = 0{\cdot}02$) and a relative error of 2 % at $M_s = 8{\cdot}0$ ($dM_s = 0{\cdot}16$). We did not go beyond $M_s \approx 8{\cdot}0$, as in similar previously conducted experiments in the same facility (Law & Glass 1971) the high-quality optical test-section windows were burned.

The initial pressure P_0 was measured with an oil manometer just after admitting the test gas. This was measured to an accuracy of dP_0 (torr) = $1{\cdot}40 \times 10^{-5}H$ (mm) + 0·08, which gives an error of 0·5 % ($dP_0 = 0{\cdot}08$) at 15 torr. (Note 15 torr corresponds to $H \approx 194$ mm.) The pressure was kept at 15 torr for the runs with $M_s = 3{\cdot}7$, 4·7 and

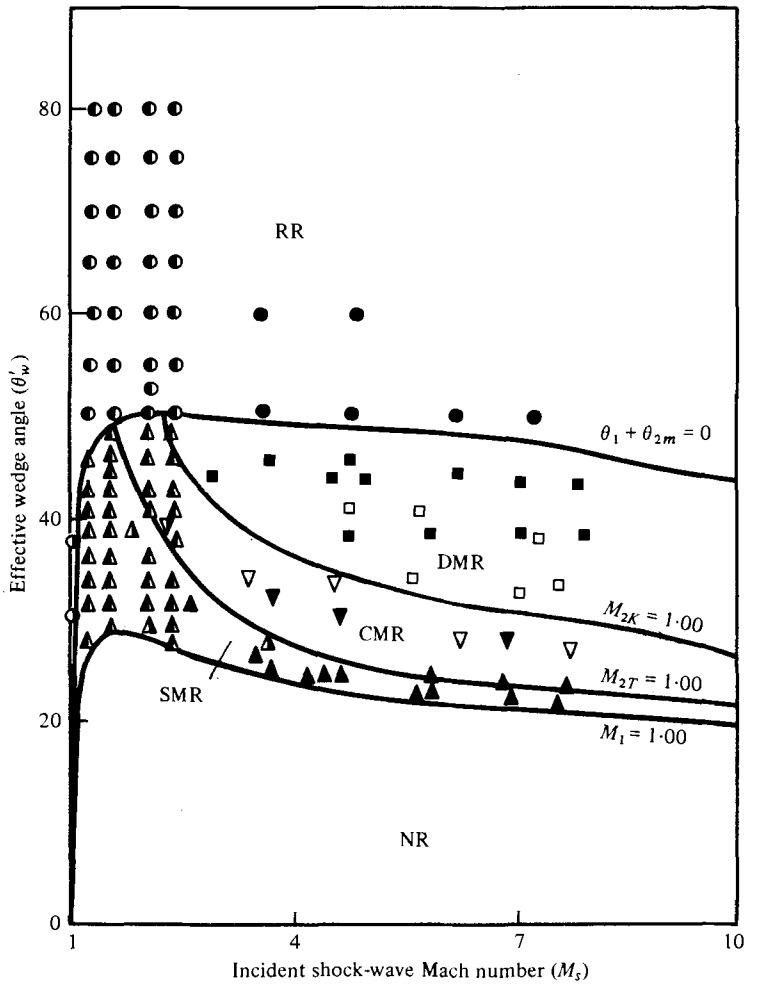

FIGURE 18. Experimental verification of oblique shock-wave reflexion analysis (pseudo-stationary frame of reference). Imperfect nitrogen $P_0 = 15$ torr, $T_0 = 300$ K. ◭, ◐, air (Smith 1945); ▽, ▲, ◑, air (White 1951); □, △, ▽, ○, oxygen (Law & Glass 1971); ■, ▼, ▲, ●, nitrogen (Ben-Dor & Glass 1978). Note the term reflexion is used since the results are plotted in the pseudo-stationary (θ'_w, M_s) plane.

6·0; 10 torr for $M_s = 7{\cdot}0$ and 8·0; 50 torr for $M_s = 2{\cdot}0$. The driving gases used to obtain the shock-wave Mach numbers with the given initial pressures were He, H_2 and CO_2, respectively. The initial driver and test-gas temperatures T_0 were usually in the range 295–299 K, and measured to an accuracy of 0·1 K. A detailed report of results is given by Ben-Dor (1978*b*).

In addition to our results, we used the experimental data of Smith (1945) for $M_s = 1{\cdot}25$, 1·51, 2·10 and 2·40 in air as well as the data obtained by White (1951) in air and Law & Glass (1971) in oxygen, as shown in figure 18 (a reproduction of figure 6 for $P_0 = 15$ torr). Note that two points from Smith's experimental data for RR lie slightly below the analytical boundary for RR. We believe that this slight disagreement is probably due to Smith's use of air. The 20 % oxygen would lower the boundary due to vibrational excitation.

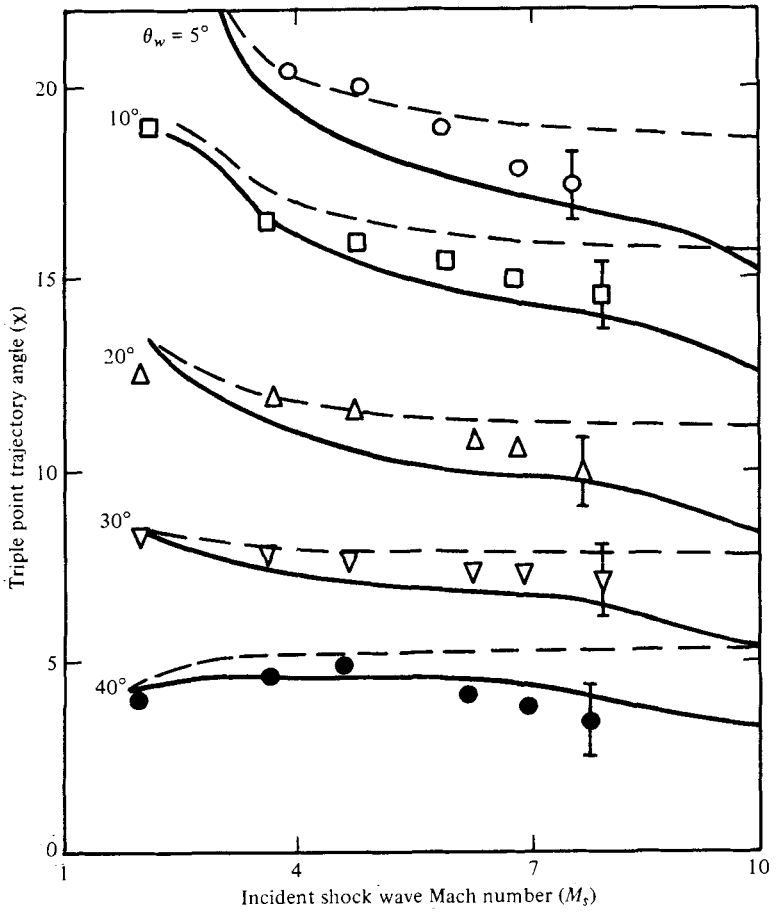

FIGURE 19. Verification of χ *vs.* M_s with θ_w and comparison with experiments. ——, imperfect nitrogen, $P_0 = 15$ torr, $T_0 = 300$ K; – – –, perfect gas $\gamma = \frac{7}{5}$ (all data points from Ben-Dor & Glass 1978).

Shock-wave reflexion configurations that are reported by Smith (1945) to be SMR in the range $2{\cdot}10 \leqslant M_s \leqslant 2{\cdot}42$ appear to lie in the region that corresponds to CMR (figure 18). However, a careful check of Smith's report reveals that he observed that, 'for strong shocks [his strongest shock was $M_s \approx 2{\cdot}42$] a reversal of curvature [in the reflected shock wave] develops' and, furthermore, 'the portion of the reflected shock near the triple point then appears to be straight'. This we believe corresponds to CMR. It is clear that although he had noticed a CMR configuration, he referred to it as a SMR rather than propose a new type of reflexion, since these two configurations, except for the kink in R, are quite similar in appearance. When White (1951) discovered DMR, the importance of CMR was recognized as a different type of reflexion. However, in White's report CMR is still considered as SMR. Excellent agreement can be seen with the no reflexion (NR) boundary line. Our analytical line $M_{2K} = 1{\cdot}00$ for the termination of CMR and the formation of DMR agrees very well with experiment.

Our data in figure 19 tests the method of predicting χ (in nitrogen) which was subtracted from figure 6 to obtain figure 13. It is seen that agreement with experiments

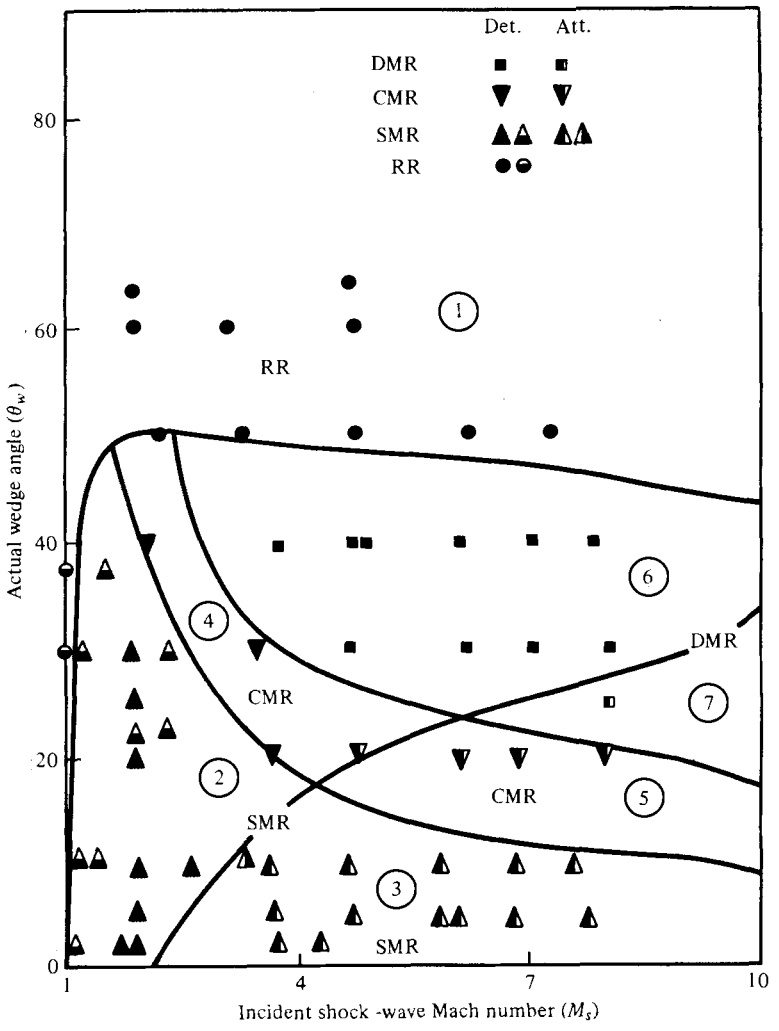

FIGURE 20. Experimental verification of analysis of seven domains and their transition boundaries of non-stationary oblique shock-wave diffraction. ◒, ▲, ◭, air (data from White 1951); ●, ■, ◧, ▼, ▽, ▲, ◭, nitrogen (Ben-Dor & Glass 1978); ——, imperfect nitrogen, $P_0 = 15$ torr, $T_0 = 300$ K. Note the term diffraction is used where both elements of shock reflexion and wedge-flow deflexion can be identified in the photographs.

for wedge angles $\theta_w > 5°$ is reasonably good. All experimental points in this region lie within $\pm 1°$ from their predicted values. However, for $\theta_w \leqslant 5°$ agreement becomes progressively worse as θ_w decreases. Note that Law & Glass (1971), who developed this method for predicting χ, found it to be good only in the range $20° \leqslant \theta_w \leqslant 45°$ (in oxygen). However their solution was graphical while the present one is analytical. Note that for $\theta_w < 40°$ the actual values of χ are larger than those predicted. In this range all the data points fall between the predicted perfect and real-gas values.

Our experimental-data points (in nitrogen) and White's in air are shown in figure 20 (a reproduction of figure 13) as a test of our analysis of the shock-wave diffraction processes in non-stationary flows. It is seen that all of the experimental-data points lie inside their predicted regions.

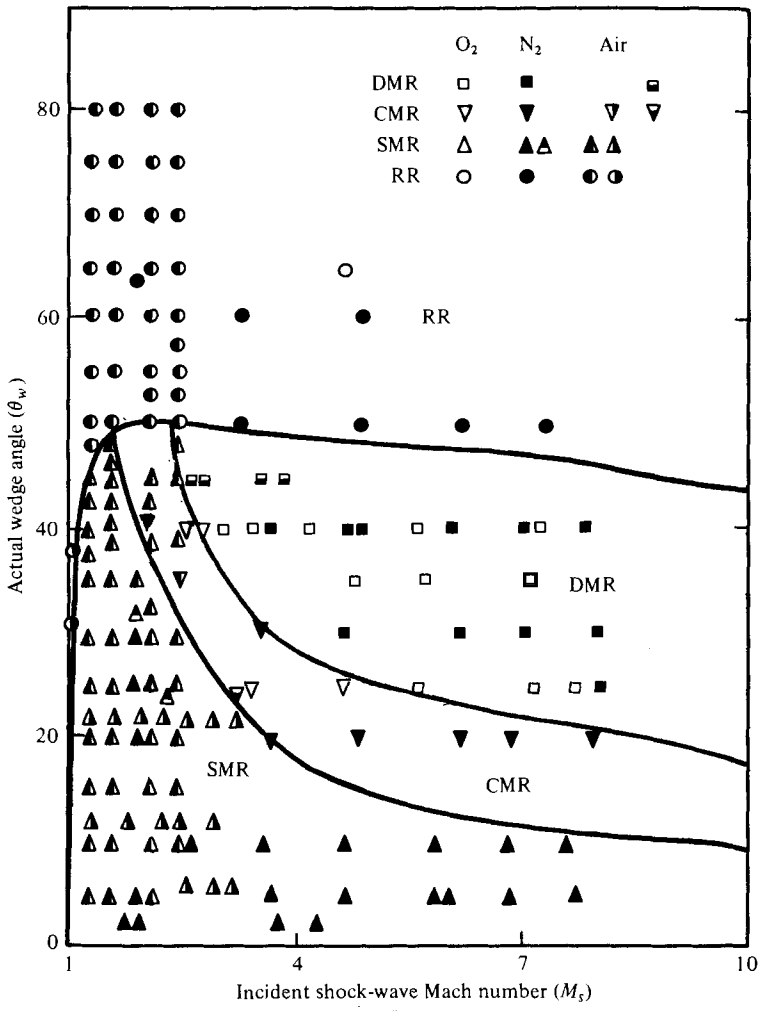

FIGURE 21. Experimental verification of analysis of oblique shock-wave reflexion for diatomic gas. Lines are for imperfect nitrogen, $P_0 = 15$ torr, $T_0 = 300$ K. ◭, ◐, air (data from Smith 1945); ▽, ◭, ◑, air (White 1951); □, ▽, △, ○, oxygen (Law & Glass 1971); ⬓, ▽, air (Bazhenova *et al.* 1976); ◬, nitrogen (Bazhenova *et al.* 1976); ■, ▼, ▲, ●, nitrogen (Ben-Dor & Glass 1978).

The data from Smith (1945), White (1951) and Bazhenova *et al.* (1976) in air, Law & Glass (1971) in oxygen and Bazhenova *et al.* (1976) and ours in nitrogen are shown in a combined plot on figure 21 (a reproduction of figure 6 with χ subtracted) in order to check the acceptability of our analysis for the diatomic gases, nitrogen, oxygen and air. All the data points that lie outside their predicted regions have been discussed previously. Two experiments (present and one from Law & Glass 1971) with $\theta_w = 40°$ and $M_s = 2{\cdot}00$ and $2{\cdot}56$ respectively, in the region where Smith (1945) reported SMR result in CMR. This substantiates our previous remarks that these experiments by Smith are CMR not SMR. Many more data points from White (1951) could have been used. However, since they fall in their predicted regions, they were omitted for clarity. It can be concluded that our analysis of the seven regions and their transition

boundaries for non-stationary oblique shock wave reflexion in a diatomic gas has been substantiated by experiments conducted by a number of researchers. Many additional details can be found in Ben-Dor (1978*a*, *b*).

4. Conclusions

An analysis was presented of the domains and the transition boundaries of non-stationary oblique shock wave reflexions for perfect and imperfect nitrogen in the (M_s, θ_w) plane. It was shown that seven regions exist for a diatomic gas consisting of the basic four types of regular, single-Mach, complex-Mach and double-Mach reflexions. The transition boundaries depend on the incident shock Mach number M_s and the reflexion wedge angle θ_u for a perfect gas and additionally on the initial temperature T_0 and pressure P_0 for a real gas. Unlike steady flows in supersonic wind tunnels where only regular and single-Mach reflexions can be observed, non-stationary flows in shock tubes give rise to the two additional complex and double-Mach reflexions. The fundamental reason lies in the fact that non-stationary shock-wave diffraction consists of two elements. One is the shock-wave reflexion process at the wedge surface and the other is the deflexion of the flow induced by the moving shock wave over the wedge. This flow can be subsonic, transonic and low supersonic. The deflexion of the supersonic flow over the wedge produces attached or detached bow waves. The deflexion processes give rise to the two additional types of non-stationary oblique shock-wave reflexions.

The analysis was substantiated by 58 interferometric experiments conducted at present and those of Law & Glass (1971) in the UTIAS 10×18 cm Hypervelocity Shock Tube as well as many other data in nitrogen, oxygen and air from several sources. It has brought new order and understanding of the various results from the different researchers. All the results fall into the predicted seven domains separated by their transition boundaries.

Two outstanding problems remain, namely a more accurate analytical formulation for finding the triple-point-trajectory angle χ and a better analytical method of predicting the location of the kink in a CMR or the second triple point of a DMR. Essentially, this means a solution for the second triple-point-trajectory angle χ' (figure 1*d*).

The very comprehensive isopycnic data are the first since the early pioneering work of White (1951) who first discovered the four types of reflexion. The results provide an important base for testing available and future computational codes describing such complex flows. Although existing numerical methods can satisfactorily predict the gross features of the wave systems and shock shapes for regular and single-Mach reflexions, they are as yet unsatisfactory for predicting the isopycnics of the flow (Ben-Dor & Glass 1978). No computational data presently exist for complex and double-Mach reflexions. Undoubtedly such codes will evolve in the near future.

The personal discussions with Dr H. G. Hornung and the private communications with Dr L. F. Henderson on regular and Mach reflexions are very much appreciated. We thank Prof. S. Molder for some constructive comments. The financial assistance received from the U.S. Air Force under grant AF-AFOSR-77-3303 and from the National Research Council of Canada is gratefully acknowledged.

REFERENCES

AULD, D. J. & BIRD, G. A. 1976 *A.I.A.A. Paper* 76–322.

BARGMANN, V. 1945 *Nat. Res. Defence Committee. App. Math. Panel*, no. 108. 2R.

BAZHENOVA, T. V., FOKEEV, V. P. & GVOZDEVA, L. G. 1976 *Acta Astronautica*, **3**, 131.

BEN-DOR, G. 1978*a* *UTIAS Rep.* no. 232.

BEN-DOR, G. 1978*b* *UTIAS Rep.* no. 237.

BEN-DOR, G. & GLASS, I. I. 1978 *A.I.A.A. J.* **16**, 1146.

BLEAKNEY, W. & TAUB, A. H. 1949 *Rev. Mod. Phys.* **21**, 584.

FLETCHER, C. H. 1951 *Dept Phys., Princeton Univ. Tech. Rep.* II-4.

FLETCHER, C. H. & TAUB, A. H. 1951 *Rev. Mod. Phys.* **23**, 271.

GLASS, I. I. & LIU, W. S. 1978 *J. Fluid Mech.* **84**, 55.

GLASS, I. I., LIU, W. S. & TANG, F. C. 1977 *Canadian J. Phys.* **55**, 1269.

GLASS, I. I., MARTIN, W. A. & PATTERSON, G. N. 1953 *UTIAS Rep.*, no. 2.

GLASS, I. I. & PATTERSON, G. N. 1955 *J. Aero. Sci.* **22**, 73.

GVOZDEVA, L. G., BAZHENOVA, T. V., PREDVODITELEVA, O. A. & FOKEEV, V. P. 1969 *Acta Astronautica*, **14**, 503.

GVOZDEVA, L. G., BAZHENOVA, T. V., PREDVODITELEVA, O. A. & FOKEEV, V. P. 1970 *Acta Astronautica*, **15**, 503.

HENDERSON, L. F. 1964 *Aero. Quart.* **15**, 181.

HENDERSON, L. F. & LOZZI, A. 1975 *J. Fluid Mech.* **68**, 139.

HORNUNG, H. G. 1977 Private communication during visit to UTIAS.

HORNUNG, H. G., OERTEL, H. & SANDEMAN, R. J. 1979 *J. Fluid Mech.* **90**, 541.

JONES, D. M., MARTIN, P. M. E. & THORNHILL, C. K. 1951 *Proc. Roy. Soc.* A **209**, 238.

KAWAMURA, R. & SAITO, H. 1956 *J. Phys. Soc. Japan* **11**, 534.

KUTLER, P. & SHANKAR, V. 1977 *A.I.A.A. J.* **5**, 197.

LAW, C. K. 1970 *UTIAS Tech. Note*, no. 150.

LAW, C. K. & GLASS, I. I. 1971 *CASI Trans.* **4**, 2.

LIEPMANN, H. W. & ROSHKO, A. 1957 *Elements of Gasdynamics*. Wiley.

LIU, W. S., WHITTEN, B. T. & GLASS, I. I. 1978 *J. Fluid Mech.* **87**, 609.

MACH, E. 1878 *Akad. Wiss. Wien* **77**, II, 1228.

MOLDER, S. 1960 *UTIAS Tech. Note*, no. 38.

MOLDER, S. 1976–1978 Private communication.

MOLDER, S. 1979 *CASI Trans.* (to be published).

NEUMANN, J. VON 1963 *Collected Works*, vol. 6. Pergamon Press.

PARKS, E. K. 1952 *UTIAS Rep.*, no. 18.

SCHNEYER, G. P. 1975 *Phys. Fluids* **18**, 000.

SEEGER, R. J. & POLACHEK, H. 1943 *Navy Dept Bureau of Ordnance, Re.* 2c, *Washington, D.C. Explosive Res. Rep.* 13.

SEMENOV, A. H., SYSHCHIKOVA, M. P. & BEREZKINA, M. K. 1970 *Sov. Phys. Tech. Phys.* **15**, 795.

SHANKAR, V., KUTLER, P. & ANDERSON, O. 1977 *A.I.A.A. J.* **16**, 4.

SMITH, L. G. 1945 Photographic investigation of the reflection of plane shocks in air. *OSRD Rep.* 6271.

TAUB, A. H. 1947 *Phys. Rev.* **72**, 51.

WHITE, D. R. 1951 *Dept Phys., Princeton Univ. Tech. Rep.* II-10.

WHITE, D. R. 1952 *Proc. 2nd Midwestern Conf. Fluid Mech.*

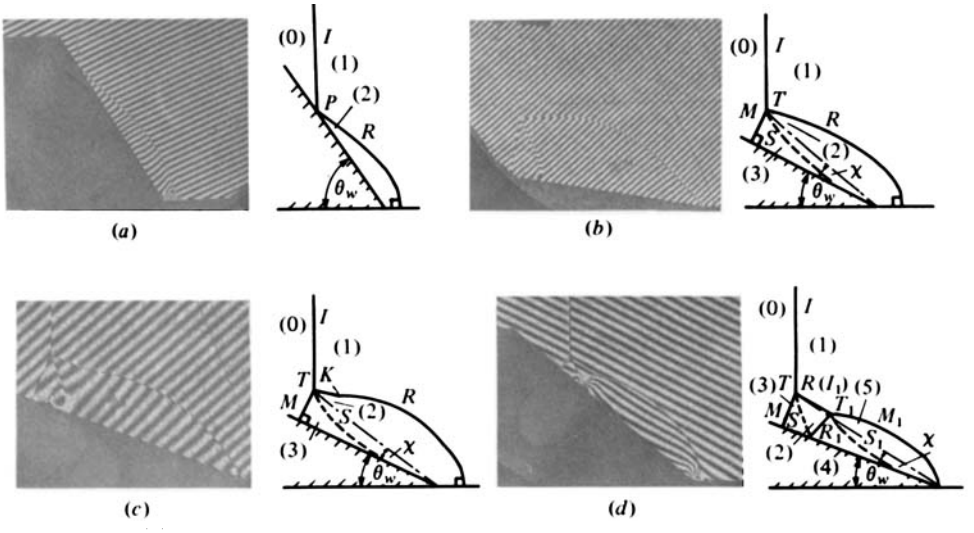

FIGURE 1. Illustration of four possible oblique shock-wave reflexions. (Interferograms are on the left and explanatory sketches on the right.) The interferograms ($\lambda = 6943$ Å) were taken with a 23 cm diameter Mach–Zehnder interferometer in the UTIAS 10×18 cm Hypervelocity Shock Tube for nitrogen at an initial pressure $P_0 \approx 15$ torr and temperature $T_0 \approx 300$ K. I, I_1, incident shock waves; R, R_1, reflected shock waves; M, M_1, Mach stems; S, S_1, slipstreams; T, T_1, triple points; χ, χ', triple-point trajectory angles; (0)–(5), thermodynamic states. (*a*) Regular reflexion (RR), wedge angle $\theta_w = 60°$, shock Mach number $M_s = 4{\cdot}68$. (*b*) Single-Mach reflexion (SMR), $\theta_w = 10°$, $M_s = 4{\cdot}72$. (*c*) Complex-Mach reflexion (CMR), $\theta_w = 20°$, $M_s = 6{\cdot}90$. (*d*) Double-Mach reflexion (DMR), $\theta_w = 40°$, $M_s = 3{\cdot}76$.

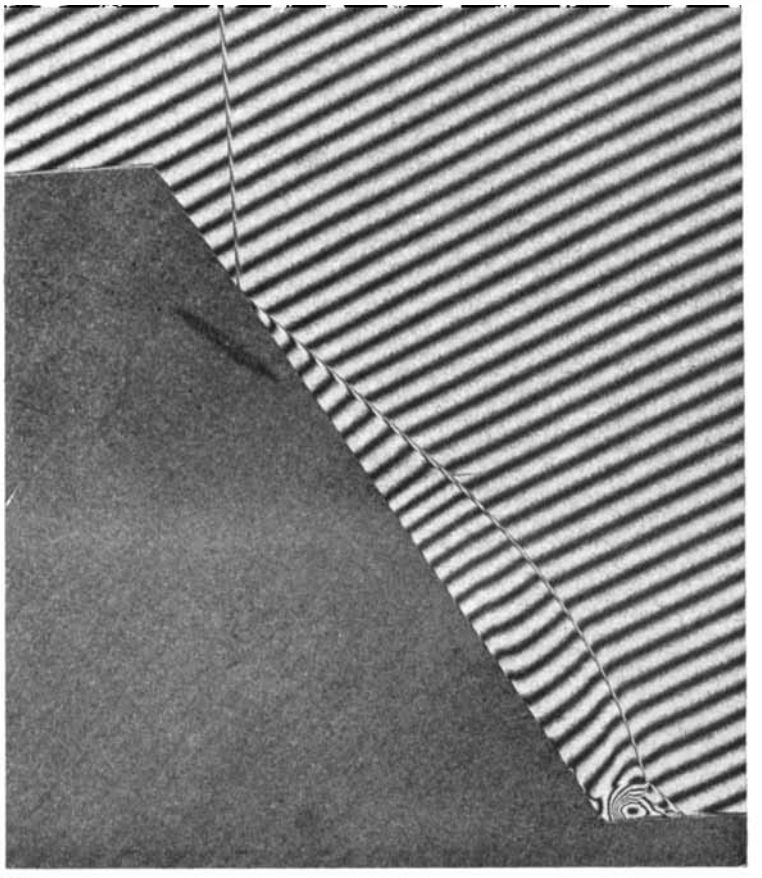

(*a*)

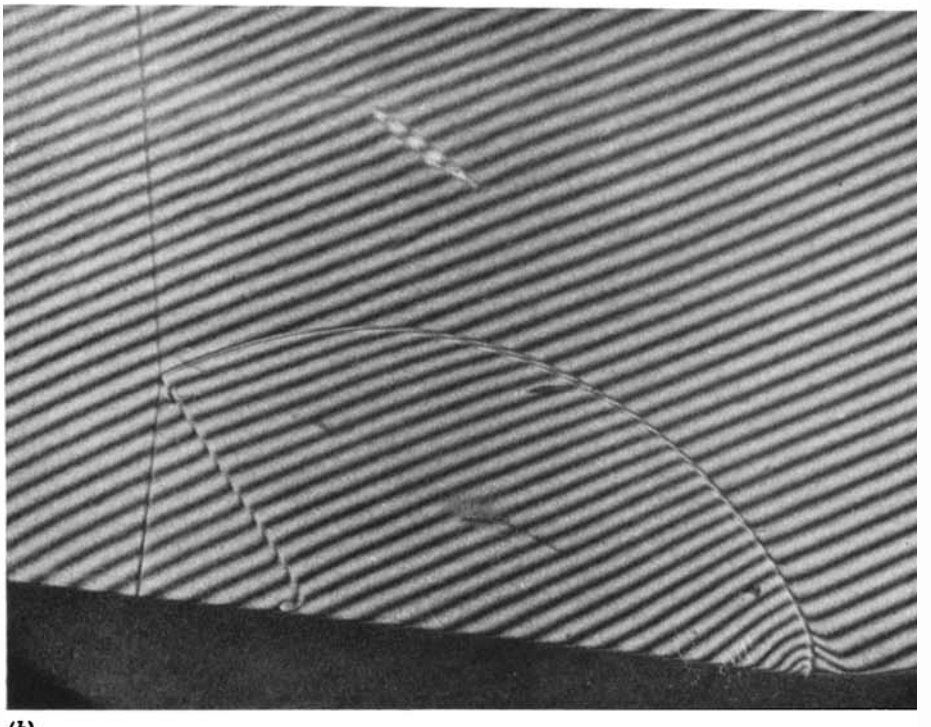

(*b*)

FIGURE 14 (*a*, *b*). For legend see plate 5.

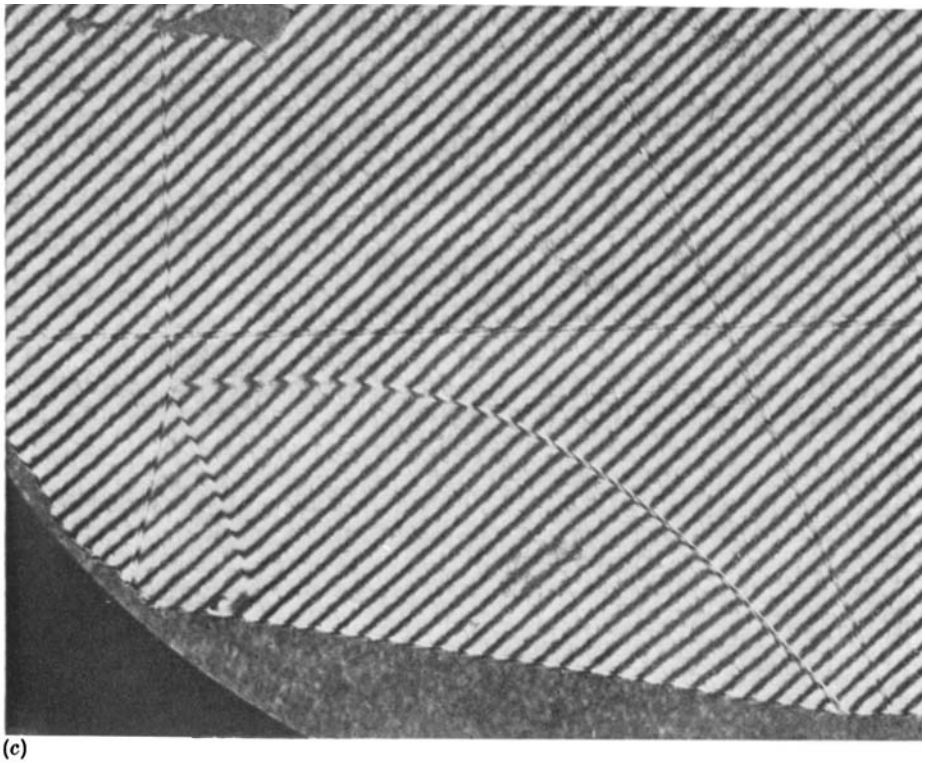

(*c*)

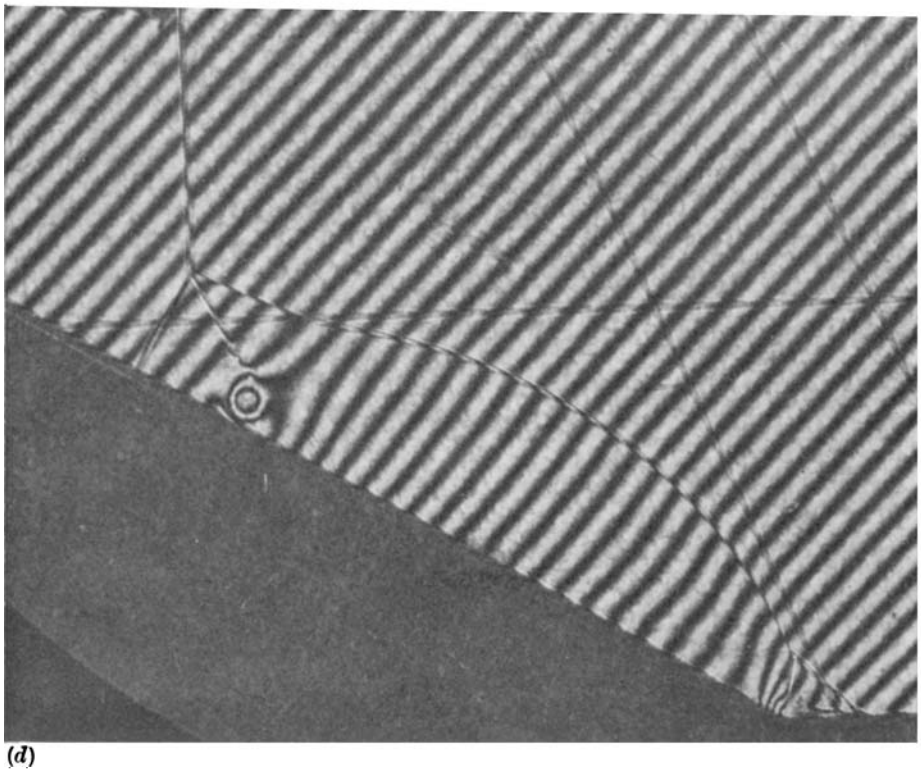

(*d*)

FIGURE 14 (*c*, *d*). For legend see plate 5.

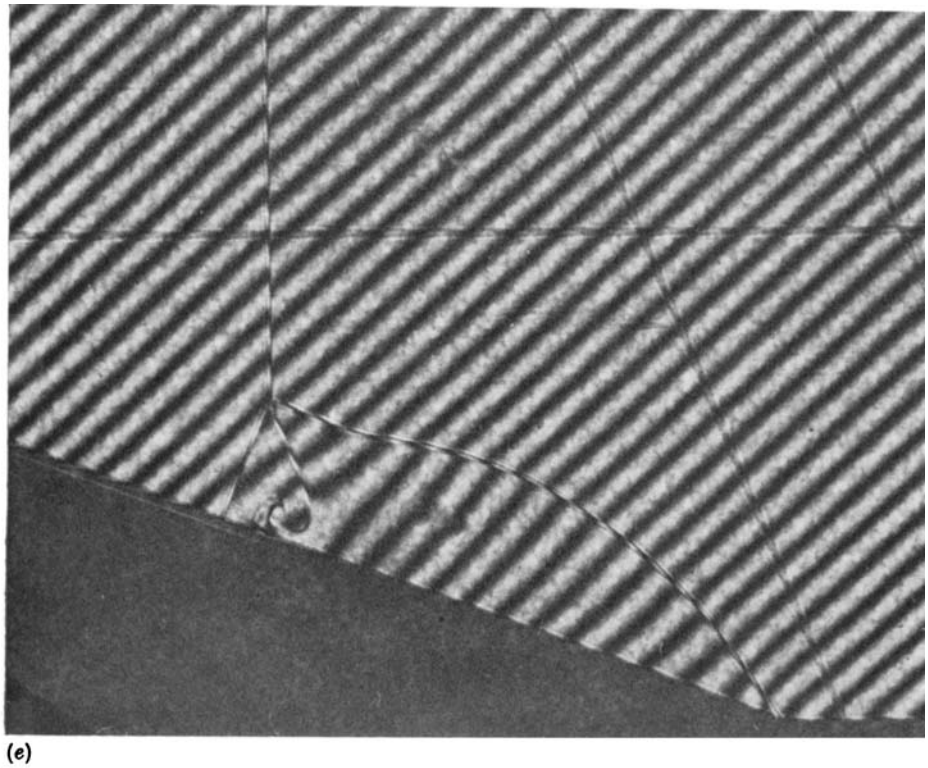

(*e*)

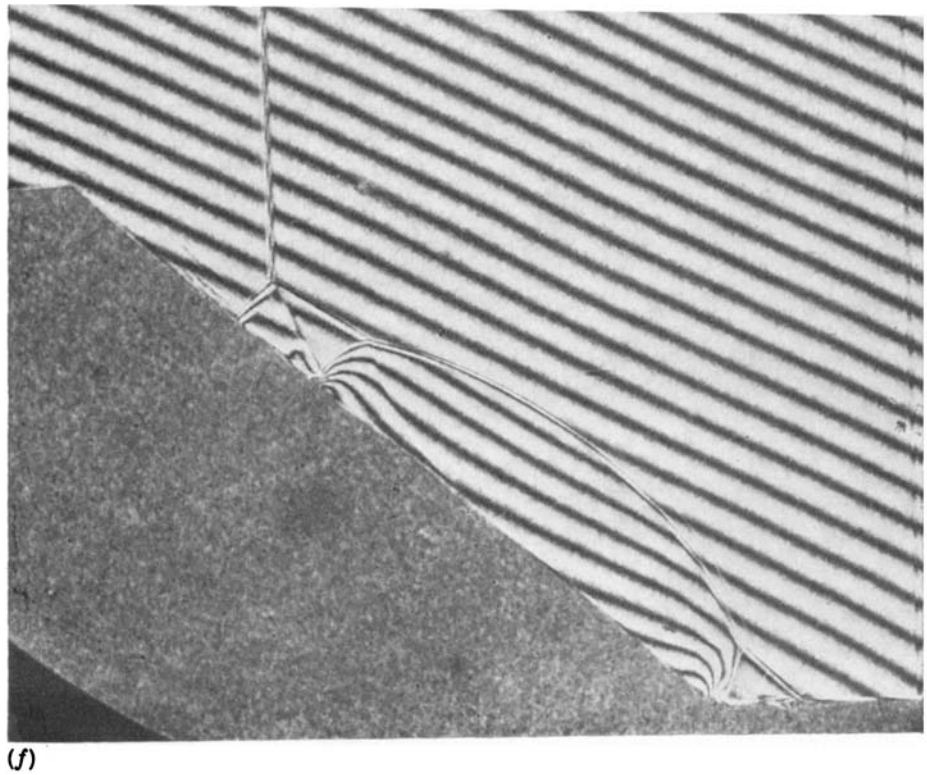

(*f*)

FIGURE 14*e*, *f*. For legend see plate 5.

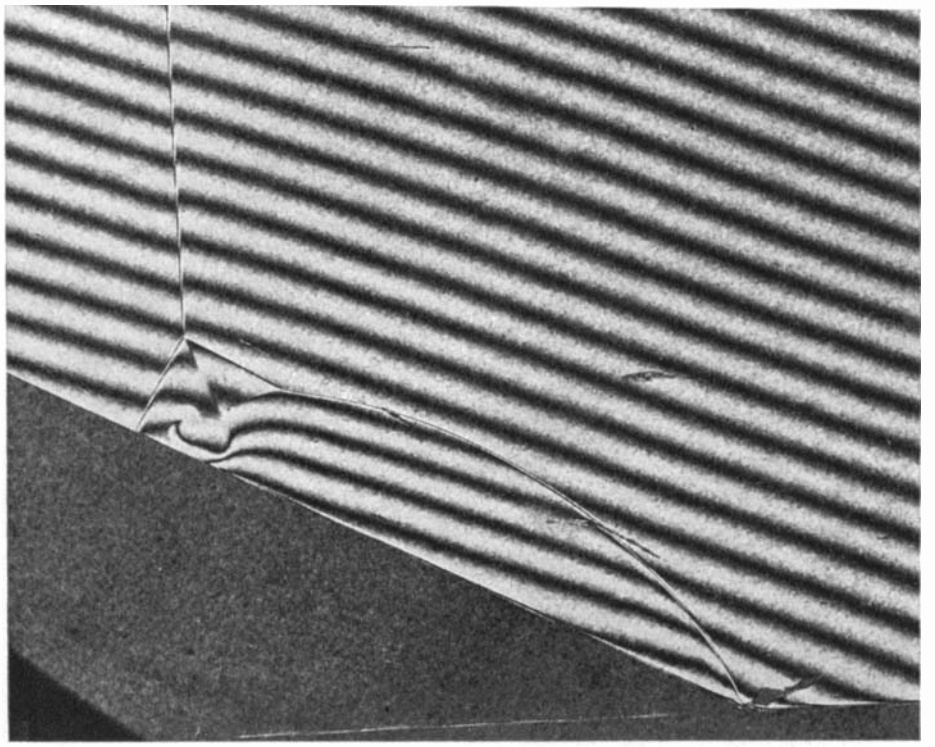

(*g*)

FIGURE 14. Interferograms of seven different oblique shock-wave diffractions in nitrogen in non-stationary flows. Plates (*a*)–(*g*) correspond to regions (1)–(7) of figure 13 ($\lambda = 6943$ Å). (*a*) $M_s = 4{\cdot}68$, $\theta_w = 60{\cdot}00°$, $P_0 = 15{\cdot}31$ torr, $T_0 = 298{\cdot}1$ K. (*b*) $M_s = 2{\cdot}61$, $\theta_w = 10{\cdot}00°$, $P_0 = 37{\cdot}00$ torr, $T_0 = 297{\cdot}8$ K. (*c*) $M_s = 4{\cdot}72$, $\theta_w = 10{\cdot}00°$, $P_0 = 15{\cdot}00$ torr, $T_0 = 295{\cdot}0$ K. (*d*) $M_s = 3{\cdot}74$, $\theta_w = 30{\cdot}00°$, $P_0 = 15{\cdot}27$ torr, $T_0 = 297{\cdot}3$ K. (*e*) $M_s = 6{\cdot}90°$, $\theta_w = 20{\cdot}00°$, $P_0 = 10{\cdot}12$ torr, $T_0 = 295{\cdot}8$ K. (*f*) $M_s = 3{\cdot}76$, $\theta_w = 40{\cdot}00°$, $P_0 = 15{\cdot}34$ torr, $T_0 = 297{\cdot}4$ K. (*g*) $M_s = 8{\cdot}06$, $\theta_w = 26{\cdot}56°$, $P_0 = 5{\cdot}11$ torr, $T_0 = 298{\cdot}2$ K.